Low-cost autonomous chambers enable high spatial and temporal resolution monitoring of soil CO_2 efflux across landscapes

This is a non-peer-reviewed preprint submitted to EarthArXiv. The manuscript has been submitted to Agricultural and Forest Meteorology.

Journal: Agricultural and Forest Meteorology

Manuscript type: Research Paper

Author names: Jonathan Gewirtzman[1,2,*], Ashley Keiser[3], Matthew A. Nieland[3], Corey Palmer[3,4], Vatsal Patel[5], Elizabeth Forbes[1,6,7,*]

Author affiliations:

[1] Yale University, School of the Environment; New Haven CT, USA

[2] Stanford University, Department of Earth System Science, Stanford Doerr School of Sustainability; Stanford CA, USA

[3] University of Massachusetts Amherst, Stockbridge School of Agriculture; Amherst MA, USA

[4] Keuka College, Division of Natural Sciences and Mathematics; Keuka Park NY, USA

[5] Yale University, School of Engineering and Applied Science; New Haven CT, USA

[6] Hudson Carbon; Hudson NY, USA

[7] University of Michigan, School for Environment and Sustainability; Ann Arbor MI, USA

Co-corresponding authors: Jonathan Gewirtzman*, Department of Earth System Science, Stanford Doerr School of Sustainability, Stanford University, 473 Via Ortega, Stanford, CA

94305, USA (jgewirtz@stanford.edu); Elizabeth Forbes*, 515 Prospect St., Hudson, NY 12545, USA (forbeselizabeth.s@gmail.com).

Keywords: Respiration; Chambers; Sensors; Replication; Heterogeneity; Intercomparison; Forest

Abstract

Soil CO_2 efflux is a central component of ecosystem carbon budgets, but the cost and logistics of measuring it often force a trade-off between spatial coverage and temporal resolution. Manual survey chambers can sample many locations but only occasionally, whereas automated chambers measure continuously but are costly and tethered to line power and a shared analyzer, which limits them to a few chambers at one site. Fluxbot 2.0 is a low-cost (about US$400 per unit), autonomous chamber designed for continuous, distributed soil CO_2 flux measurements without external power or infrastructure. To test whether distributed Fluxbot arrays reproduce reference measurements, we deployed two eight-unit arrays alongside an established automated chamber network in two forest stands at Harvard Forest, USA, for one month, processing fluxes from both systems with the same code. Over 305 compared hours, Fluxbot system means averaged 0.3% below autochamber means, a difference no larger than that between disjoint chamber subsets of the same system, as expected for systems sampling different collars. The chamber-adjusted difference was statistically equivalent within 20%. Daily means correlated at $r = 0.85$ across 15 qualifying days (hourly $r = 0.72$). Averaged across stands, the gap-filled October budget was about 2% lower for Fluxbots. Fluxbot fluxes were depressed during likely sensor wetting, which the units' humidity records could flag. Low-cost arrays thus gave reference-like mean fluxes in both stands and make dense replication affordable. Because each unit is self-contained, extending

arrays across sites, land-cover types, environmental gradients, or treatments requires only more units.

Highlights

- Low-cost autonomous chamber means were within 0.3% of reference autochambers
- Daily means correlated at r = 0.85 across 15 qualifying days
- Both systems showed late-day flux maxima and similar between-chamber variation
- A shared-control outage stopped one autochamber array for 164 hours
- Dense, affordable arrays enable soil CO_2 monitoring across heterogeneous landscapes

1. Introduction

Soil respiration, the efflux of carbon dioxide (CO_2) from soil (hereafter soil CO_2 efflux), is the largest terrestrial source of CO_2 to the atmosphere, accounting for the majority of gross terrestrial ecosystem emissions (Friedlingstein et al. 2025) at over 90 Pg C annually (Bond-Lamberty and Thomson 2010; Hashimoto et al. 2023). As an essential component of ecosystem carbon budgets, accurate measurements of this flux help describe and model feedbacks between terrestrial ecosystems and the atmosphere. Soil CO_2 efflux varies from diel to seasonal time scales, from centimeters to kilometers (Vargas et al. 2011; Bradford and Ryan 2008; Premke et al. 2016), and with topography, vegetation, and disturbance (Rodeghiero and Cescatti 2008), so accurately capturing it requires high spatial and temporal resolution as well as broad spatial coverage.

Many questions that depend on this flux are spatial. Microtopography, individual plant species, and species assemblages create localized hotspots of element cycling (Jevon et al. 2023; Keiser et al. 2024), variation in soil moisture and chemistry creates hot spots and hot moments of soil fluxes (Gachibu Wangari et al. 2023; Leon et al. 2014; Savage et al. 2014), and urbanization and ecosystem fragmentation alter spatial patterns of soil CO_2 efflux along overlapping gradients

(Garvey et al. 2022; Reinmann et al. 2020). Animals, from earthworms to selectively browsing moose, add further heterogeneity (DeCarlo and Caylor 2019). Asking how wild (e.g., Ohashi et al. 2007; Saunders et al. 2023) and domestic animals (e.g., Ondier et al. 2020), and changes in their communities (Forbes et al. 2019), shape soil carbon cycling requires spatially distributed or dense measurements (Ferraro and Lienau 2025; Forbes et al. 2023; Schmitz et al. 2018; Risch et al. 2013). These processes also vary with daily (e.g., Forbes et al. 2023; Tang et al. 2005; Savage et al. 2009; Savage et al. 2014) and seasonal (Giasson et al. 2013; Davidson et al. 2006) cycles in soil conditions and with climate (Raich et al. 2002; Carey et al. 2016; Huang et al. 2020). Soils are central to agricultural carbon mitigation (Paustian et al. 1997; Paustian et al. 2000; Paustian et al. 2016), and measurement-based carbon offset and credit programs need soil CO_2 efflux data resolved across space and time (Kim et al. 2025) in place of current estimation-based methods (Novick et al. 2022).

Existing methods trade resolution in space against resolution in time. Manual survey chambers with precision gas analyzers capture detailed spatial patterns, but cost and labor limit how often sites can be revisited and the extent over which measurements can be compared. Automated chambers provide continuous records, but they often cost more than US$20,000 per system, and multiplexed chambers are tethered by tubing, wiring, and line power to a shared analyzer, pump, and power supply. Automated deployments are therefore limited to a few chambers at one location (Savage and Davidson 2003; Liang et al. 2003), so continuous chamber records remain sparse and weakly replicated (Bond-Lamberty et al. 2020; Görres et al. 2016). Although eddy covariance towers measure ecosystem-scale fluxes continuously over large areas, they lack the spatial resolution to identify drivers of flux variability (Hollinger et al. 2004). Manual chambers thus favor spatial coverage and automated chambers temporal resolution, but none of these

methods combines high spatial and temporal resolution with broad spatial extent (Forbes et al. 2023; Pan et al. 2024).

Distributed arrays of autonomous, low-cost devices offer a way around this trade-off. They give up some precision in each measurement for much greater replication and coverage, complementing rather than replacing high-precision systems. Low-cost CO_2 sensors have been used to increase the replication of gas-exchange measurements (Macagga et al. 2024; Al Hamwi et al. 2024; Nguyen et al. 2025), in portable, open-source systems (Carbone et al. 2019), in automated tree stem chambers (Brändle and Kunert 2019; Helm et al. 2021), and in soil flux chambers validated against reference systems (Curcoll et al. 2022), and diffusion-based designs without pumps have an established precedent in soil flux measurement (Risk et al. 2011). Low cost and simple deployments also widen access to flux monitoring in understudied ecosystems and regions with limited research infrastructure (Forbes et al. 2023). Most of these low-cost systems have been validated as sensors in the laboratory, or as individual chambers compared with a reference analyzer or handheld survey chamber (e.g., Harmon et al. 2015; Macagga et al. 2024; Al Hamwi et al. 2024; Zeng et al. 2026), including multiplexed low-cost systems (Gagnon et al. 2016; Cui et al. 2026). However, none, to our knowledge, has been tested as a full system deployed at scale. It therefore remains unknown whether an array of independent chambers, running unattended in the field for weeks, reproduces the site means, budgets, temporal dynamics, and spatial variability measured by an established reference system, and what its failure modes are.

We developed the Fluxbot, a low-cost, autonomous soil CO_2 flux chamber, for distributed monitoring across landscapes. Each unit has its own sensor, battery, and cellular telemetry and needs no external power or site infrastructure, so Fluxbots can be concentrated within a site to

resolve spatial variability or spread across land-cover types, environmental gradients, and experimental treatments. Forbes et al. (2023) introduced an earlier version of the Fluxbot, with a workflow for building and deploying arrays, and Pan et al. (2024) described the Fluxbot 2.0 hardware and the performance of its electronics and communications in engineering conference proceedings. Here we report the first evaluation of Fluxbot 2.0 as a measurement system in the field, and of its ability to resolve ecological patterns in soil CO_2 efflux. We evaluate two arrays of eight Fluxbot 2.0 units against two long-established arrays at Harvard Forest (Petersham, MA, USA), each of six automated chambers (hereafter autochambers) coupled by tubing to a high-precision flow-through infrared gas analyzer (IRGA), which have monitored soil CO_2 efflux in two contrasting forest stands since 2015–2016. We ask: (i) Do the two systems agree in mean flux, monthly total, diel cycle, and temperature response? (ii) Is any difference between the systems larger than the difference between groups of collars measured by the same system? (iii) How many chambers are needed to estimate a site mean with a given precision? (iv) What are the failure modes of each system?

2. Methods

2.1 Study site

We worked in two eastern hemlock (*Tsuga canadensis* L.) forest stands approximately 0.4 km apart at the Harvard Forest Long Term Ecological Research (LTER) Site in Petersham, Massachusetts, USA (stand 1: 42.541500, −72.174624; stand 2: 42.539069, −72.178541; Fig. S1). Both were infected by the hemlock woolly adelgid (*Adelges tsugae*) in 2009 and were selected for long-term monitoring because of their contrasting responses to infection: the Bigelow Brook stand ("stand 1") continues to resemble an uninfected hemlock stand, whereas the hemlock tower

stand ("stand 2") has lost much of its hemlock and now has higher plant diversity in the overstory and understory. Six automated, multiplexed soil chambers have monitored soil CO_2 efflux in each stand since 2015–2016 (Fig. 1).



Fig. 1. *Field deployment of soil CO_2 flux monitoring systems at Harvard Forest. Fluxbot 2.0 units and autochambers in a hemlock stand. The larger pneumatically operated autochambers are connected by tubing to a central control box containing the IRGA, whereas each Fluxbot 2.0 operates independently with an integrated CO_2 sensor and servo-actuated lid. The inset shows a Fluxbot 2.0 unit. The two systems were co-located within each stand but measured separate collars. (Photo credit: JG)*

2.2 Harvard Forest autochambers

The autochambers are installed on collars of schedule 80 PVC pipe (inner diameter 28.7 cm; 646 cm^2), about 7 cm long and inserted about 3 cm into the soil. The six autochambers in each stand are arranged in a circle around a control box, which holds the IRGA (LI-800 in stand 1 and LI-840 in stand 2; LI-COR, Lincoln, NE, USA), a pump, a datalogger, a relay controller, and a power supply. The chambers are plumbed to solenoid valves at the control box, which route compressed air to and from the pistons that open and close the lids, and sampled air from the chambers to the IRGA. All six chambers in a stand therefore share one pump, analyzer, pneumatic system, and power supply, which runs on AC line power. The chambers are activated

in sequence every five minutes, so each chamber is measured every 30 minutes. Each measurement starts with 45 s with the lid open and air drawn at 1 L min^{-1}; the lid then closes, CO_2 is recorded at 1 Hz for 4 min 15 s, and the lid reopens so that the chamber vents. System volumes (collar, lid, and 274 cm^3 of tubing and analyzer volume) ranged from 9,000 to 10,450 cm^3, giving effective headspace heights of about 14–16 cm (Table 1; component details in Supplementary Information [SI] Section S1).

2.3 Fluxbot array

We deployed eight Fluxbot 2.0 chambers in each stand, six among the autochambers and two as backups in case of failure, distributed evenly through the area covered by each autochamber array; data from all eight units in each stand were analyzed. Each Fluxbot is a commercially available PVC sewer cap with a hinged lid, screwed onto its own PVC collar (schedule 40; 10.2 cm inner diameter; 81 cm^2; inserted about 4 cm into the soil), so the two systems did not share collars or soil footprints. A servo motor opens and closes the lid once an hour: the lid stays open for one minute (54:00–55:00) while ambient CO_2 is recorded, closes for five minutes (55:00–60:00) while CO_2 accumulates, and then reopens so that the chamber vents. Fluxbot chamber volume averaged 768 cm^3, an effective headspace height of about 9.5 cm.

Each Fluxbot has a Senseair K30 nondispersive infrared (NDIR) CO_2 sensor in the lid, read about every 6 s. The K30 samples the headspace by diffusion, without the tubing and pump of a flow-through analyzer, from inside a fitted polytetrafluoroethylene (PTFE) envelope that protects it from liquid water (Blackstock et al. 2019). Uncorrected K30 readings differ between units by several to about 20 ppm and drift with temperature and time in use (Yasuda et al. 2012; Martin et al. 2017), but a flux depends on the sensor's gain, not on its offset. A Sensirion SHT-30 sensor (air temperature and relative humidity, RH) and an LPS22 sensor (barometric pressure) sit next to

the K30. Each unit runs for up to 13 days on its own battery pack, and a Particle Boron microcontroller operates the sensors and lid and transmits data hourly over the cellular (LTE) network, so units share no component with one another. Fluxbot 2.0 extends the battery life of the original design (Forbes et al. 2023) from about 24 h to more than 300 h and adds wireless data transmission and improved weatherproofing, at about US$400 in parts per unit; Pan et al. (2024) describe its engineering in full.

Table 1. Characteristics of the two measurement systems as deployed at Harvard Forest.

	Autochamber	Fluxbot 2.0
Units per stand	6	8
Collar area; insertion depth	646 cm^2; ~3 cm	81 cm^2; ~4 cm
System volume; effective headspace height	9,000–10,450 cm^3; 14–16 cm	768 cm^3; 9.5 cm
Headspace mixing	Pumped through analyzer (1 L min^{-1})	Diffusion only
CO_2 sensor	IRGA (LI-840 / LI-800), shared by all chambers	NDIR K30 in PTFE envelope, one per chamber
Sampling rate	1 Hz	~0.17 Hz (one reading per ~6 s)
Measurement frequency	Every 30 min per chamber	Every 60 min per unit
Closure length; fit window used	4 min 15 s; 220 s	5 min; 3 min (57:00–60:00)
Lid actuation	Pneumatic pistons, shared compressed air and solenoid manifold	Servo motor, one per unit
Power	AC line power, shared	Battery pack per unit (up to ~13 days)
Data	Datalogger at control box	Hourly LTE transmission per unit
Ancillary sensors	—	Air temperature, RH, pressure inside the lid
Approximate cost	>US$20,000 per multiplexed system	~US$400 in parts per unit

2.4 Fluxbot–autochamber comparison

Both systems ran concurrently in each stand from 2 to 31 October 2023. Each autochamber array required its own control box, analyzer, compressed-air supply, and line power, with every

chamber within tubing distance of the box; the Fluxbots required none of these and were placed among the autochambers only so that the two systems could be compared. Because each system measured its own collars, the comparison is between co-located arrays rather than between instruments sampling the same soil, and any difference between systems combines instrument and chamber effects (Davidson et al. 2002; Pumpanen et al. 2004) with spatial variation among collars. We therefore compare stand and system means, and compare the systematic difference between systems with the variability among collars within each system. This design evaluates complete measurement systems as deployed rather than sensor accuracy, which Pan et al. (2024) reported. Terms used throughout are defined in Table 2.

Table 2. Terms used in this paper.

Term	Meaning
Closure	One flux measurement: the chamber lid closes and CO_2 accumulates in the headspace (5 min for Fluxbots, 4 min 15 s for autochambers).
System	Fluxbot 2.0 or autochamber.
Array	The chambers of one system in one stand; each system has two arrays (stands 1 and 2).
Stand mean	Hourly mean flux of an array, computed when at least three of its chambers reported.
System mean	Mean of a system's two stand means.
Compared hours	Hours in which both systems had at least three chambers reporting in each stand. We used these hours to compare full-array system means.
Offset	System mean of Fluxbots minus that of autochambers over compared hours.
Chamber failure	A closure with too few records to fit a flux, or in which the chamber did not seal or vent, or (autochambers) an hour in which the shared control system failed (Section 2.7).
RH-screened (main dataset)	Closures that passed quality control, minus Fluxbot closures with in-chamber relative humidity ≥ 99% before closure (wet sensor).
As deployed	The same without removing wet-sensor closures (SI Section S4.3).

2.5 Environmental data

Hourly air temperature, 10-cm soil temperature, and precipitation came from the Fisher Meteorological Station at Harvard Forest (HF001; Boose and VanScoy 2025), in an open field 1.1–1.5 km from the stands. Station pressure at the stands was taken from the LPS22 sensors inside the Fluxbot chambers (hourly median of the units in each stand) for both systems; it averaged 976 hPa, 3.9% below the sea-level-reduced HF001 value. Soil temperature is also logged at the autochambers (HF293; Finzi et al. 2026), but by a single probe per stand, at the interface of the organic and mineral horizons. These probes tracked HF001 closely ($r = 0.93$ and 0.81 in stands 1 and 2) but differed from it in level by −0.7 and +4.4 °C, which a single probe cannot separate from its placement. To provide a common index of seasonal and diel temperature change for both systems, we therefore used HF001 soil temperature at 10 cm. This supports comparisons between systems and stands, but not in-stand estimates of temperature sensitivity.

2.6 Flux calculation

Fluxes from both systems were calculated from the raw concentrations with the same code, the goFlux R package (Rheault et al. 2024), using chamber volume, collar area, air temperature (inside the chamber for Fluxbots; HF001 for autochambers) and station pressure. For Fluxbots, the first two minutes after lid closure were discarded, because CO_2 reaches the K30 through its envelope with a delay (median 48 s), and fluxes were fitted over 57:00–60:00; for autochambers, which close after a 45-s open-lid period, fluxes were fitted over 220 s starting 30 s after closure. As CO_2 accumulates in a closed chamber, it weakens the diffusion gradient from the soil, so the concentration curve bends and a straight line fitted to it underestimates the flux; the bend is stronger in a small headspace. For each closure, goFlux therefore fits both a linear model and the curvilinear Hutchinson–Mosier model (HM; Hutchinson and Mosier 1981), which estimates the

flux at the start of the fit window, and selects between them with explicit criteria (Hüppi et al. 2018; Rheault et al. 2024). goFlux chose HM for 90% of Fluxbot and 80% of autochamber closures, and the selected flux exceeded the linear flux by a median of 16% for Fluxbots and 2% for autochambers. We used model selection for both systems and report linear fits as a sensitivity analysis (SI Section S2.3). Autochamber fluxes published in the Harvard Forest Data Archive (HF293; Finzi et al. 2026) are calculated with a different procedure; we recalculated them so that both systems were processed identically (SI Fig. S3). Instrument precision, error codes, and a test of the Fluxbot's lower sampling rate are described in SI Section S2.

2.7 Quality control and datasets

Quality control used the same rules for both systems (details in SI Section S2.5). A closure was removed as a chamber failure if it had too few records to fit a flux; if CO_2 declined or did not accumulate significantly (linear-slope test, $p < 0.05$), which at October fluxes indicates a chamber that did not seal; or if the lid was stuck shut, so that the chamber did not vent between closures. We classified a saturated Fluxbot episode as a stuck lid when its median open-lid CO_2 anomaly (relative to the other units in the stand) exceeded 500 ppm; for autochambers, the same threshold applied to the starting concentration of each closure. Because the six autochambers in a stand share one pump, pneumatic system, and power supply, we also excluded an autochamber array-hour when at least three distinct chambers had a declining slope, a nonsignificant slope, or a linear-fit R^2 below 0.5 during that assigned hour. Isolated spikes in each chamber's flux series were removed with a robust screen (median ± 5 median absolute deviations). We did not remove individual closures for a weak fit alone, because goodness-of-fit thresholds preferentially remove small fluxes. After applying the linear-fit QC rules, we retained selected fluxes with their sign, including values below the minimum detectable flux.

The main dataset also removes Fluxbot closures with in-chamber RH ≥ 99% in the minute before closure, which indicates that the K30 or its envelope was likely wet (Pan et al. 2024); we call it the RH-screened dataset, and the dataset without this step "as deployed" (Table 2; SI Section S4.3). To identify how moisture affects the K30, we ran PTFE-covered and uncovered sensors beside a laser-based reference analyzer (M-GGA-918, ABB–Los Gatos Research, San Jose, CA, USA; hereafter LGR) in two laboratory tests, through dry periods, wetting of the PTFE envelope, and wetting of bare sensors (SI Section S4.1).

Measurement accounting counts intended closures at each system's programmed interval (one per Fluxbot and two per autochamber per hour) for every installed unit. Measurement success is the share of hours in which a unit contributed a flux to the main dataset, and replicated coverage is the share of hours with at least three units of a system reporting in a stand.

2.8 Statistical analysis

Times are local (Eastern Daylight Time, UTC−4). We assigned each closure to the nearest clock hour using the start of its fit window, then averaged autochamber fluxes (two per hour) within chamber and assigned hour. "Stand means" were computed for hours in which at least three chambers of a system reported, and the "system mean" as the mean of the two stand means; hours in which both systems had at least three chambers reporting in each stand were "compared hours" (Table 2). Daily system means required at least 12 compared hours in a local calendar day. Agreement of hourly and daily system means was quantified with the Pearson correlation r; Lin's concordance correlation coefficient (CCC; Lin 1989; Akoglu 2018), which combines correlation with agreement in level; the mean difference (offset); and the root-mean-square difference as a percentage of the mean autochamber flux (nRMSE). We show the relationship with an ordinary least-squares (OLS) fit and Bland–Altman limits of agreement (Bland and Altman 1986).

Because the two systems measured different collars, we compared their disagreement with that between disjoint subsets of three chambers per stand drawn from the same system (200 distinct pairings of subsets per comparison), reporting P, the probability that a cross-system pairing disagreed more than a within-system pairing (0.5 = indistinguishable). Pairings share chambers, so they describe the range of possible collar groupings rather than independent replicates; formal inference on the system difference comes from the GAM, which treats chambers as replicates.

Stand and system effects were tested with a generalized additive model (GAM; mgcv; Wood 2017) with stand and system as parametric terms, smooth terms for hour of day and 10-cm soil temperature, and a random intercept for chamber. Because a non-significant difference does not show that two systems agree, we also tested whether the system effect was small enough to be negligible, with two one-sided tests (TOST; Schuirmann 1987): two systems are equivalent within a chosen margin when the 90% confidence interval of their difference lies entirely within that margin. We fitted the GAM to screened chamber-hours and expressed equivalence margins as percentages of the mean across all screened autochamber chamber-hours. We report the smallest margin at which equivalence could be declared, and test ±10% for reference. Cumulative CO_2-C over 2–31 October was computed for each stand and system by gap-filling missing hours with a GAM of flux on soil temperature and hour of day (SI Fig. S4), with 95% intervals from resampling chambers.

Diel cycles were characterized from hour-of-day means over common stand-hours, those with at least one reporting chamber of each system in the same stand. Temperature sensitivity was expressed as Q_{10}, the fitted factor change in flux for a 10 °C increase, and estimated from exponential fits of each system's pooled hourly fluxes on 10-cm soil temperature over the common stand-hours. For chambers with at least 100 qualifying chamber-hours, we also fitted

log flux against soil temperature using fluxes above 0.5 μmol m^{-2} s^{-1}. We compared the geometric mean chamber Q_{10} between systems and resampled chambers within stands for the ratio interval. Spatial heterogeneity was summarized with Gini coefficients (Gini 1912) and coefficients of variation (CV) of chamber-mean fluxes, from which we estimated the number of chambers needed for the 95% confidence interval of a monthly stand mean to fall within ±10% and ±20%. Further details and sensitivity analyses are in the SI (Sections S2–S5). All analyses were conducted in R (R Core Team 2024).

3. Results

3.1 Fluxes, temporal trends, and stand differences

Over the 305 compared hours, mean soil CO_2 efflux was 2.88 μmol m^{-2} s^{-1} from autochambers and 2.87 μmol m^{-2} s^{-1} from Fluxbots. Daily system means ranged from 2.1 to 3.7 μmol m^{-2} s^{-1} for autochambers and from 1.8 to 4.7 μmol m^{-2} s^{-1} for Fluxbots. Fluxes from both systems declined over the month, with multi-day fluctuations (Fig. 2a), as air temperature (Fig. 2b) and 10-cm soil temperature (from about 19 to 11 °C) fell. Three rain events (7–8, 20–22, and 29–31 October) wetted many Fluxbot sensors, and the 20–22 October event wetted most units at once. The two stands did not differ significantly: the GAM stand effect was −0.02 μmol m^{-2} s^{-1} (SE 0.31; $p = 0.95$), and stand means over compared hours differed by less than 3% in each system, in opposite directions (autochambers 2.92 and 2.84, Fluxbots 2.85 and 2.90 μmol m^{-2} s^{-1} in stands 1 and 2). For full-array agreement, we gave the two stand means equal weight.

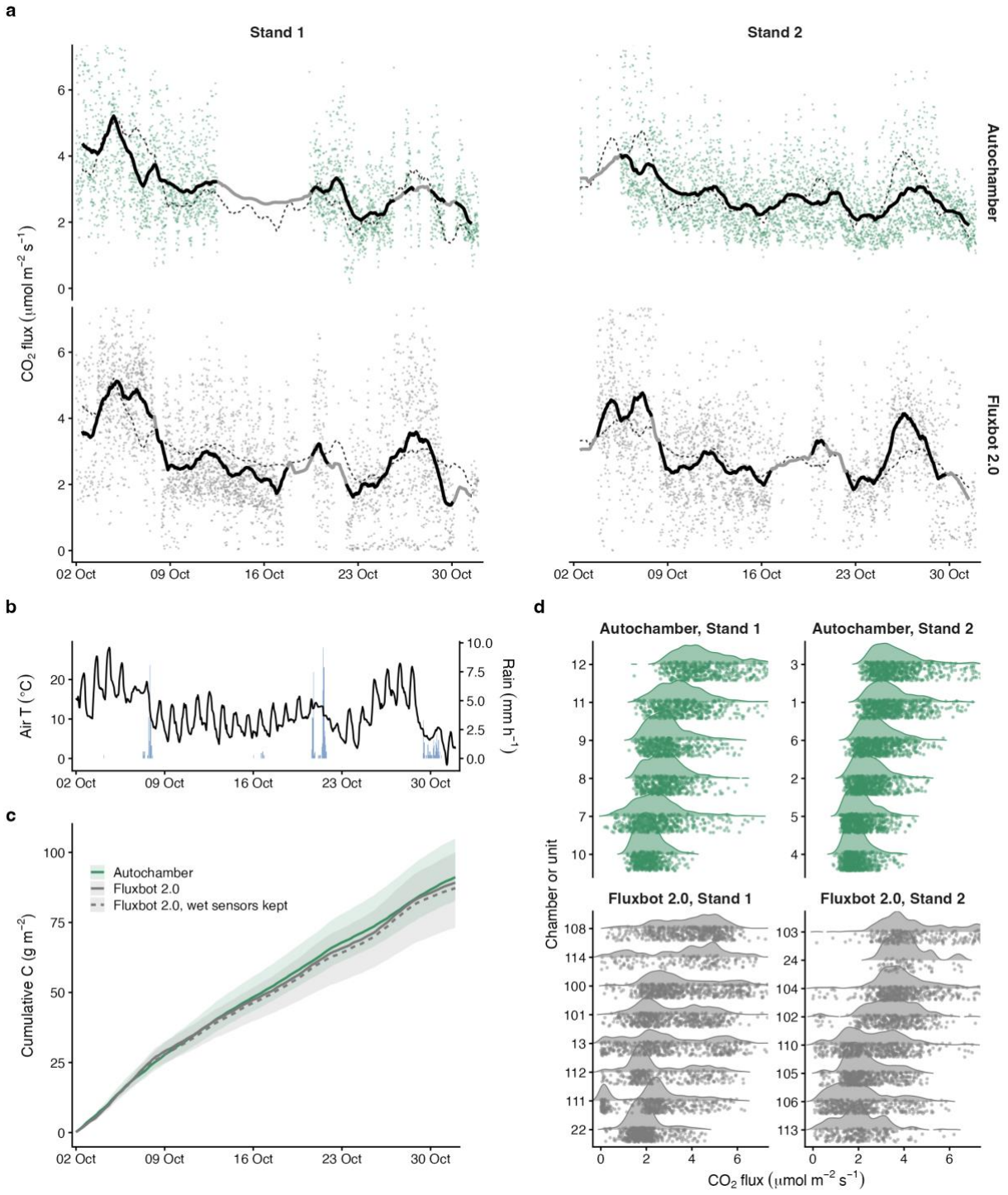


Fig. 2. *Fluxes, budgets, and chamber variation, 2–31 October 2023 (main dataset). (a) Retained chamber-hour fluxes (points; autochamber points can average two closures) for each system (rows) and stand (columns). Lines are 24-h centered means of the gap-filled stand-mean series, dark where mostly observed and light where mostly modeled; thin dashed lines repeat the other system's series for comparison. (b) Air temperature (line) and hourly precipitation (bars) at HF001. (c) Cumulative CO_2-C, gap-filled for each stand and averaged over stands; bands show 95% intervals from 100 chamber resamples; the dashed line is the Fluxbot budget with wet-sensor closures*

kept. (d) Flux distribution of each chamber (ridges) with its retained chamber-hour fluxes (points), by array; chambers are ordered by mean flux. Fluxes above the plotted range in (a) and (d) are not shown.

3.2 Agreement between systems and monthly budgets

The two systems' means tracked each other closely and did not differ in level (Fig. 3). In the compared hours, hourly means were correlated with r = 0.72 (CCC = 0.67; nRMSE = 23%) and daily means, across 15 qualifying days, with r = 0.85 (CCC = 0.74; nRMSE = 17%; SI Fig. S5). The mean offset was −0.01 μmol m^{-2} s^{-1} (−0.3%). Fluxbot system means spanned a somewhat wider range than autochamber means (Fig. 3), although fluxes varied over only a narrow range during the month. The GAM system effect, which accounts for differences among chambers, was −0.05 μmol m^{-2} s^{-1} (95% CI −0.66 to 0.56). Its 90% CI excluded differences larger than 19.2% of the mean autochamber flux but not differences of 10% (TOST p = 0.22; SI Section S3.2).

The difference in level between systems was of the size expected from sampling different collars: the median absolute offset between disjoint three-chamber subsets was 9% of the mean flux across systems and 11% within either system (P = 0.42; Fig. 3c; SI Section S3). Hourly correlation was lower across systems (median r = 0.66) than within autochambers (0.90) or Fluxbots (0.84), so short-term dynamics differed somewhat more than spatial sampling alone would explain (Section 4.2).

Integrated over the month, gap-filled efflux was 91.1 g C m^{-2} (95% CI 78.6–103.7) from autochambers and 89.2 g C m^{-2} (75.2–101.9) from Fluxbots, a ratio of 0.98 (0.81–1.18) (Fig. 2c). Fluxbot budgets were about 7% lower in stand 1 and 3% higher in stand 2. With linear fits for both systems, Fluxbot system means were 11% lower than autochamber means and the budget ratio was 0.87 (0.74–1.04), as expected from the stronger curvature of Fluxbot closures, although hourly means were more closely correlated (r = 0.81; Section 4.2; SI Section S2.3).

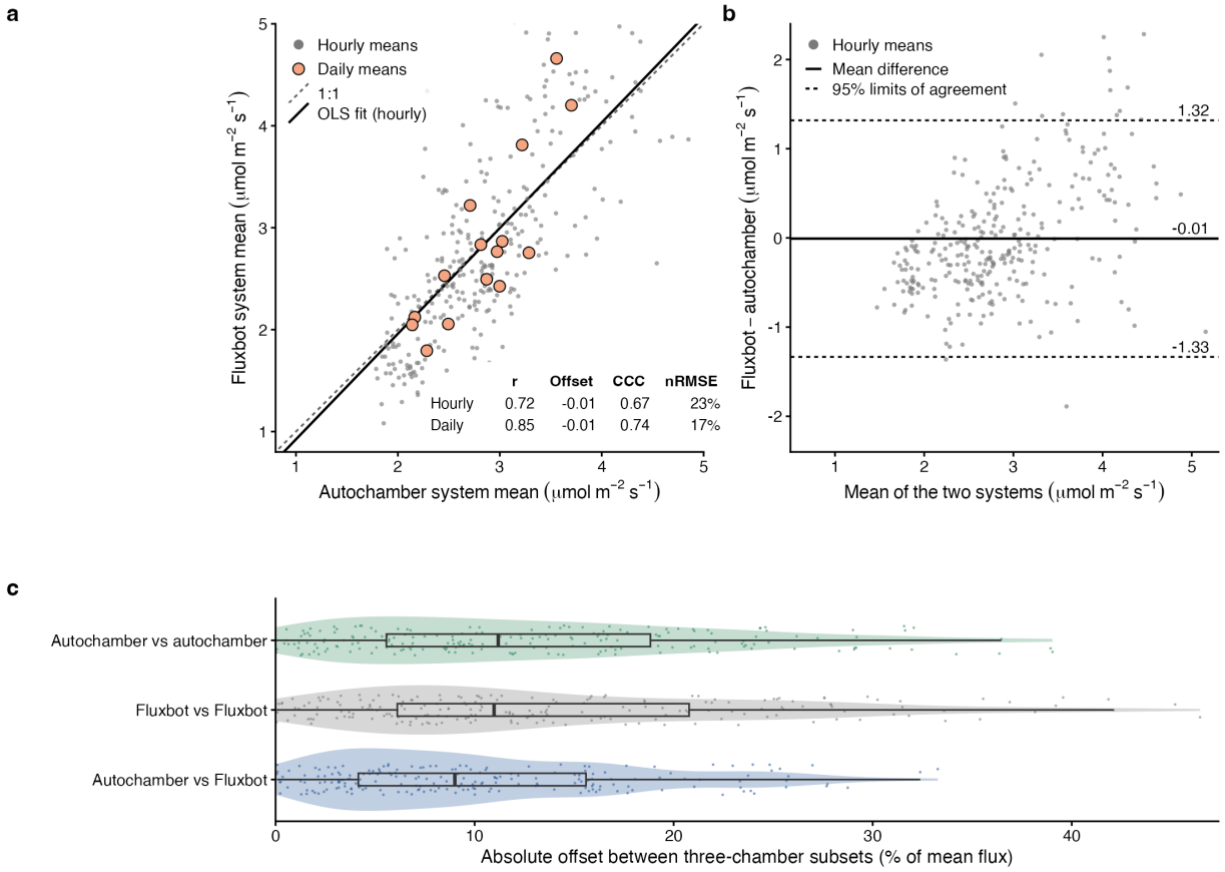


Fig. 3. *Agreement between system means (mean of the two stand means) in compared hours (main dataset). (a) Fluxbot vs autochamber hourly means; outlined points, daily means; dashed line 1:1; solid line OLS fit of hourly means. The inset gives r, offset (μmol m^{-2} s^{-1}), CCC, and nRMSE for hourly and daily means. (b) Bland–Altman plot of the same hourly means, with the mean difference and 95% limits of agreement, drawn at the same scale on both axes. A few hourly means above 5 μmol m^{-2} s^{-1} are outside the plotted range in (a). (c) Absolute offset between disjoint subsets of three chambers per stand, drawn from the same system or from different systems (spatial-null benchmark; 200 distinct pairings per comparison; each point is the offset over the whole period for one pairing, as a percentage of the mean of the two subset means; violins, distributions; boxes, quartiles). Pairings share chambers and are not independent replicates.*

3.3 Diel cycle and temperature response

Both systems detected a diel cycle with late-afternoon to evening maxima and similar amplitudes (0.79 and 0.89 μmol m^{-2} s^{-1}, or 27% and 29% of the daily mean, for autochambers and Fluxbots; Fig. 4a). Autochamber fluxes peaked at 18:00, and Fluxbot fluxes were elevated from 17:00 to midnight, with less precise hour-of-day means (median 95% CI ± 0.42 vs ± 0.30 μmol m^{-2} s^{-1}; SI Section S5.1). Over the common stand-hours (10-cm soil temperature 11.2–19.1 °C), Q_{10} from

pooled fits was 2.84 for autochambers and 3.70 for Fluxbots (Fig. 4b); the geometric mean chamber-level Q_{10} was 28% higher for Fluxbots, but with wide uncertainty among chambers (ratio 1.28, 95% CI 1.00–1.64).

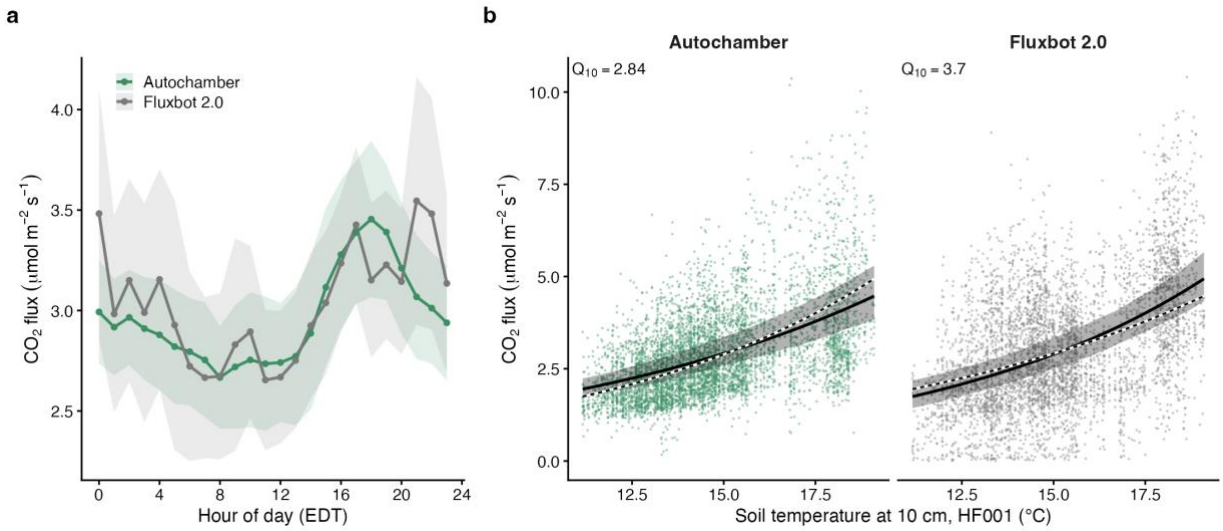


Fig. 4. *Responses to meteorological drivers, in stand-hours in which both systems reported (main dataset). (a) Diel cycle of each system: hourly means, with bands showing 95% confidence intervals across days. (b) Temperature response of each system: solid lines are exponential fits; bands are 95% intervals from resampling chambers within stands; dashed lines repeat the other system's fit for comparison.*

3.4 Spatial variability and sampling effort

Chamber-mean fluxes covered the same range in both systems (1.9–4.8 µmol m^{-2} s^{-1}; Fig. 2d), with similar between-chamber standard deviations (0.84 for autochambers and 0.89 µmol m^{-2} s^{-1} for Fluxbots). Gini coefficients of chamber-mean fluxes were low and similar (0.14 and 0.16; Fig. 5a), as were the mean within-stand CVs of chamber means (0.28 and 0.30). At the observed within-stand variability, the projected 95% CI half-width for a monthly stand mean was about 20% of the mean with 11 independent chamber locations (9–14 across the four arrays) and 10% with 35 (26–49) (Fig. 5b); these estimates rest on six to eight chambers per array.

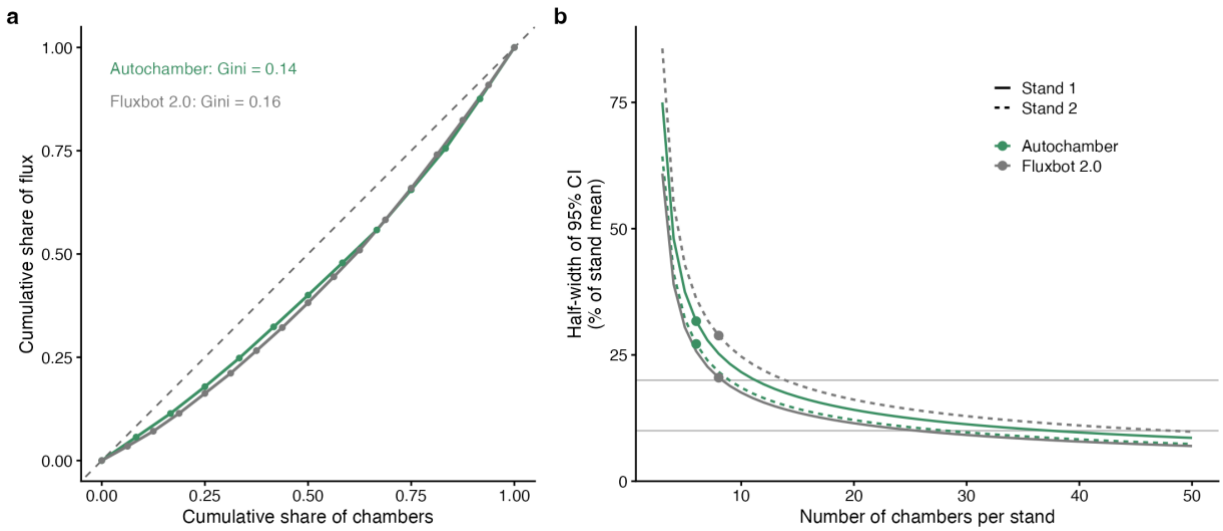


Fig. 5. *Spatial heterogeneity and sampling effort. (a) Lorenz curves and Gini coefficients of chamber-mean fluxes. Gini coefficients pool stands and use the 133 hours with at least 12 chambers reporting per system. (b) Uncertainty of a stand mean (half-width of its 95% confidence interval, as % of the mean) as a function of the number of chambers per stand, from within-stand CVs; points mark the number deployed.*

3.5 Data yield and failure modes

The Fluxbot arrays recorded 8,591 of 11,520 intended closures (74.6%), and 6,301 (54.7%) remained in the main dataset after quality control; the autochamber arrays recorded 14,353 of 17,280 (83.1%), and 13,309 (77.0%) remained (Fig. 6a). The largest Fluxbot loss occurred before flux calculation: 2,929 intended Fluxbot closures had no record. The RH screen removed 661 otherwise retained closures. Measurement success varied much more among Fluxbot units than among autochambers (Fig. 6b, c). The two systems failed in different ways (Fig. 6d). The stand-1 autochamber array produced no data for 164 h (12–19 October) and failed to seal on 5 and 25–30 October, when 870 closures were removed as whole-array failures; a further 85 closures, mostly from one chamber on 2–3 October, were removed as stuck lids. Fluxbot losses came from transmission gaps, a battery depletion across all units on 16–18 October, six units that stopped working before the end of the month, and 737 closures with stuck lids. Replicated coverage (at least three units reporting) was maintained in 81% and 70% of hours by Fluxbots in stands 1 and 2, and in 67% and 90% of hours by autochambers (Fig. 6d; SI Fig. S8).

Fluxbot fluxes were depressed during likely sensor wetting. In-chamber air was saturated in 19% of recorded unit-hours: 941 h in 65 wet-sensor episodes, mostly during rain, and 737 h in which a stuck lid kept the chamber closed. In the wet-sensor episodes (median 14 h), Fluxbot fluxes were depressed relative to autochamber fluxes: the Fluxbot/autochamber ratio fell from 0.77 in the first 2 h of an episode to 0.58 after 13–24 h, against 0.99 in dry periods. After in-chamber humidity fell below saturation, the open-lid baseline (ambient CO_2 measured with the lid open) returned to normal within 1–3 h, but the flux ratio stayed at about 0.85 for a day and then varied around the dry-period level (SI Section S4.2). The offset was −3.0% over 357 as-deployed compared hours and −0.3% over 305 RH-screened compared hours, and daily r was 0.80 and 0.85 (SI Table S2b). In laboratory tests, dry K30 sensors responded linearly between about 420 and 1,700 ppm with gains of 0.97–1.00 relative to the LGR, although they read 33–52 ppm high. Wetting the PTFE envelope made readings erratic, shifted some upward, and reduced the covered-to-uncovered slope ratio from 0.93 to 0.85. Only bare sensors failed outright (SI Section S4.1).

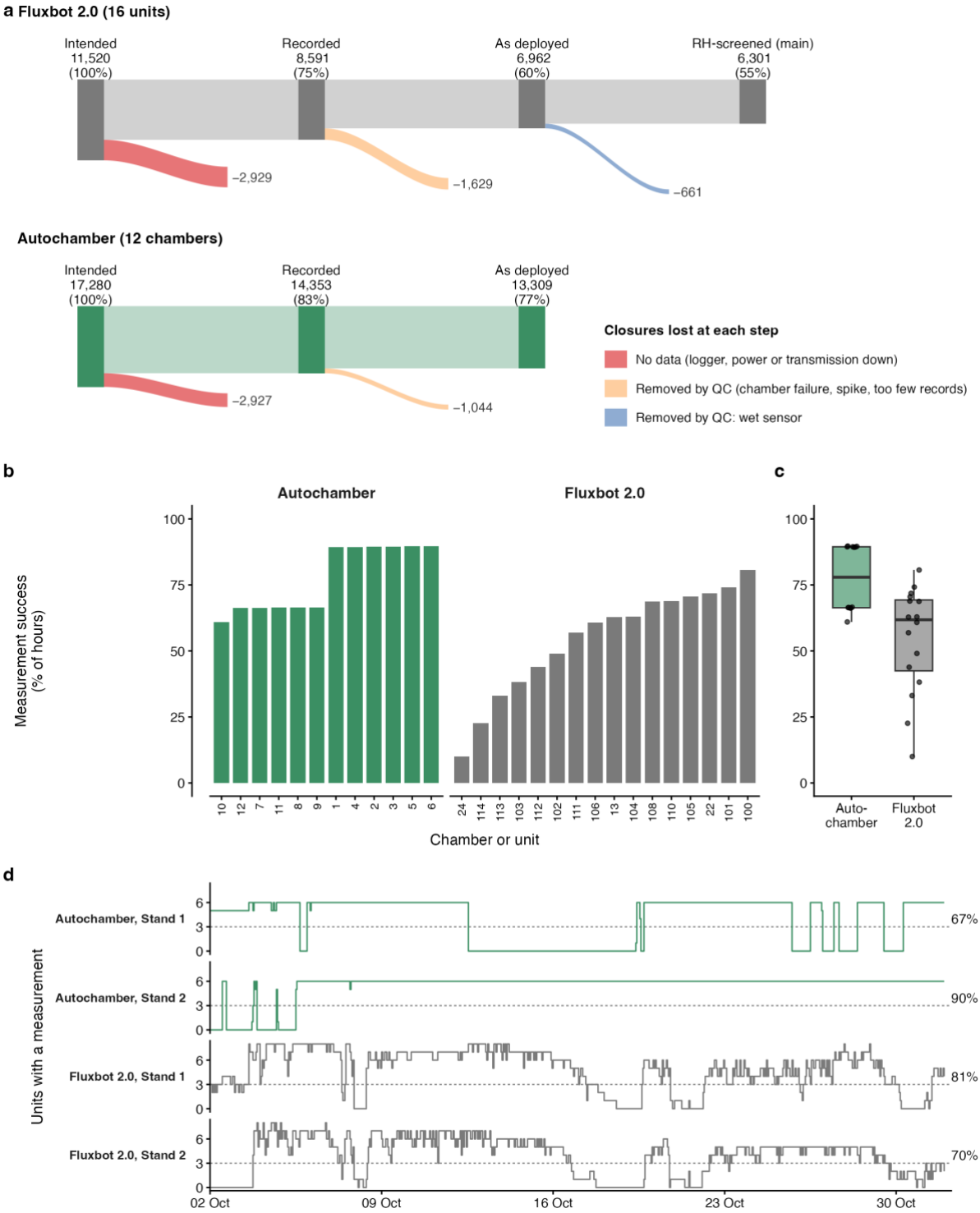


Fig. 6. *Data yield and coverage, 2–31 October 2023. (a) Closures of each system as a share of intended closures (one per Fluxbot and two per autochamber per hour): recorded closures had any data; as-deployed closures passed quality control (Section 2.7; finer steps in SI Section S2.5); the RH-screened main dataset also excludes wet-sensor closures (Fluxbots only). Ribbons show losses at each step, with the number of closures lost. (b) Measurement success of each chamber or unit (share of hours with a flux in the main dataset) and (c) its distribution in each system. (d) Number of units in each array with a measurement in the main dataset, hour by hour; the dashed line*

marks three units (replicated coverage), and the percentages give the share of hours with at least three units. Autochambers in an array share one control box and report or fail together; Fluxbot units report or fail individually. The record of every chamber is shown in SI Fig. S8a.

4. Discussion

4.1 Fluxbot arrays reproduce site-level fluxes

Across the two stands, Fluxbots reproduced the reference system's October mean and cumulative efflux more closely than its hour-to-hour variation. Differences in mean flux between systems were comparable to differences between disjoint collar subsets within a system (Fig. 3c). Earlier evaluations of low-cost chambers tested sensors in the laboratory or compared individual chambers with reference instruments (e.g., Harmon et al. 2015; Macagga et al. 2024; Zeng et al. 2026). Whole systems have been compared at the level of site means, budgets, and data coverage, but only between commercial automated systems (Görres et al. 2016) or between automated and manual chambers (Savage and Davidson 2003). This study extends that kind of system-level test to low-cost chambers deployed at scale. For site-level means and budgets over days to weeks, Fluxbot arrays can therefore complement or extend a reference network.

Fluxbot sensors were not calibrated to absolute concentrations, and did not need to be: a flux depends on the rate of change in concentration, not on its level. A sensor's gain does matter, because a slope scales with it. Uncalibrated K30s read 33–52 ppm above the reference analyzer in the laboratory but had gains of 0.97–1.00 (SI Section S4.1), and the close agreement in mean flux in the field is consistent with this. This is consistent with reports that low-cost sensors in closed-chamber accumulation measurements perform well without frequent calibration (Harmon et al. 2015); periodic span checks would guard against drift in long deployments, which is the main source of error in large low-cost NDIR networks (Yasuda et al. 2012; Müller et al. 2020).

4.2 Why hourly fluxes differ

Perfect agreement at fine temporal and spatial scales is not expected from separate sets of collars in a soil whose respiration varies at sub-meter scales (Bradford and Ryan 2008; Vargas et al. 2011; Martin and Bolstad 2009). Hourly means agreed less closely than daily means partly because model-selected fluxes are noisier (below) and because the two systems' short-term dynamics differed somewhat, plausibly through differences in collar size, insertion depth, headspace mixing, and chamber height (Davidson et al. 2002; Pumpanen et al. 2004); averaging over a day removed most of this difference.

The flux model mattered more than any other processing choice we examined (SI Table S2). With linear fits, Fluxbot means were 11% lower than autochamber means. Model selection reduced the difference to 0.3%, consistent with the stronger curvature of Fluxbot concentration traces in the small headspace; because the systems measured separate collars, not all of this difference can be attributed to either instrument. Model-selected fluxes were less precise, because the Hutchinson–Mosier fit extrapolates the slope back to the start of the fit window (standard errors 2.5–4 times those of linear fits), and these larger fit errors may have contributed to the lower hourly correlation between systems (0.72 against 0.81 with linear fits); because Fluxbot subsets with the same model selection still correlated at $r = 0.84$, real differences in short-term dynamics also contributed. Users of low-cost chambers should report the flux model and fit window and test the sensitivity of their conclusions to them.

The late-afternoon to evening diel maxima of both systems are consistent with temperature-dependent root and microbial respiration and lagged supply of recent photosynthate (Savage and Davidson 2003; Tang et al. 2005). Fluxbot fluxes rose relative to autochamber fluxes when air was warm relative to soil (SI Section S5.1). Because air inside a closed Fluxbot warmed very

little during a closure, chamber heating is an unlikely cause. Smaller collars may instead respond more to near-surface soil and litter, which warm and cool more than soil at 10 cm; this may also explain the higher, though uncertain, Fluxbot Q_{10}. Both Q_{10} values fall within the range commonly reported for temperate forest soils (Davidson and Janssens 2006), but values from a one-month deployment depend on the depth and location of the temperature record (Lloyd and Taylor 1994), here open-field soil temperature 1.1–1.5 km from the stands, and are confounded with the seasonal decline in temperature and substrate supply (SI Section S5.1), so they should not be extrapolated beyond the autumn conditions of this study.

4.3 Replication and distribution in space and time

The similar within-stand CVs of chamber means (0.28 and 0.30) and chamber-level ranges of the two systems show that both arrays captured comparable spatial variability within stands. Replication is where low-cost chambers add the most value. At the observed variability, about 11 independent chambers per stand would give a projected 95% CI half-width of 20% of a monthly mean, and about 35 chambers would reduce it to 10% (Fig. 5b), consistent with analyses of sampling design for soil respiration (Rodeghiero and Cescatti 2008; Pavelka et al. 2018) and more than the six chambers in each Harvard Forest autochamber array. At about US$400 in parts per unit, replication of this order is feasible at a fraction of the cost of a commercial autochamber system.

Distribution is the second advantage of a Fluxbot array, and this deployment demonstrates it. Covering two stands 0.4 km apart took two complete autochamber systems, each with its own analyzer, compressed air, and line power (Section 2.4). The two Fluxbot arrays needed only the units themselves: they shared no equipment, ran independently, and reported over the cellular network. Nothing in their operation depended on the stands being close together, or on the units

being grouped into arrays at all, so adding sites means adding units rather than infrastructure, within cellular coverage and reach for battery changes. Combining continuous records with spatial replication and needing no site infrastructure, distributed arrays can extend chamber networks over larger areas and into understudied ecosystems, as other low-cost sensor networks have broadened access to environmental monitoring (Harmon et al. 2015; Rundel et al. 2009; Bastviken et al. 2015), detect both fine-scale patterns and ecosystem-level trends (Bastviken et al. 2022; Jian et al. 2018), and support carbon accounting in managed systems (Novick et al. 2022). Eddy covariance towers, satellites, and airborne systems cover large areas but with less spatial specificity (Baldocchi 2003); dense chamber arrays could complement them by resolving soil efflux within tower footprints (Phillips et al. 2010). In air-quality monitoring, distributed networks of lower-precision units have greatly expanded the mapping of pollutants across cities, providing data for policymakers and communities (Castell et al. 2017; Hasenfratz et al. 2015; Dubey et al. 2024); as with the Fluxbot arrays here, they are characterized against reference instruments.

Applications extend beyond monitoring of forest carbon. In community ecology and zoogeochemistry, distributed arrays could map how animal activities, from soil invertebrates to large herbivores, create spatial patterns in carbon cycling (Forbes et al. 2019). Agricultural measurement, monitoring, reporting, and verification protocols increasingly require high-resolution soil carbon data to validate sequestration claims, particularly in heterogeneous landscapes and across extreme weather events and seasons (Burba 2025; Bradford et al. 2025). Arrays could also track the recovery of soil respiration in ecosystem restoration and its spatial pattern in fragmented urban green spaces, and their autonomy suits remote or inaccessible ecosystems where data gaps are largest.

4.4 Reliability in the field

Moisture caused the main bias in Fluxbot fluxes, as in other deployments of low-cost NDIR sensors (Blackstock et al. 2019; Müller et al. 2020), although missing records caused more data loss (Section 3.5). Laboratory tests largely rule out water vapor inside the sensor as the cause; the field depression more likely reflects liquid water on or condensation within the PTFE envelope. The envelope protected the electronics from liquid water (bare sensors sprayed with water stopped recording or returned error codes; covered sensors did not) but did not keep out water vapor, so condensation could still form inside it (SI Section S4.1). Wet covers raised readings in our laboratory tests, as for K30s encapsulated in expanded PTFE (Blackstock et al. 2019), but an offset does not change a slope; the lower field fluxes may instead reflect slowed diffusion through an envelope wetted by condensation, which brief laboratory wetting did not reproduce. The small effect of humidity alone is specific to PTFE-covered K30s over the range tested; other low-cost NDIR sensors need humidity corrections (Müller et al. 2020; Curcoll et al. 2022; but see Heger et al. 2020). After drying, the open-lid baseline returned to normal within hours, but fluxes stayed about 15% below autochamber fluxes for a day and then varied around the dry-period level, possibly in part because soils were re-equilibrating after rain. Wetting left no lasting change in response over the month (SI Section S4.2); whether repeated wetting degrades sensors over longer deployments remains to be tested. A simple, automatable rule, removing closures with in-chamber RH $\geq$ 99%, removed most of this error. Because wet periods were modestly high-flux periods, screening also lowers a gap-filled budget slightly through sampling alone: restricting the autochamber record to Fluxbot coverage lowered its gap-filled budget by 0.7% under as-deployed coverage and 1.3% under RH-screened coverage (SI Section S4.3), so the

share of wet hours should be reported with budgets. Venting or warming the sensor compartment, or a cover that sheds water, could reduce condensation in future designs.

The autochambers retained a larger share of their intended closures but were more vulnerable to complete shutdown. Because Fluxbots are independent of one another, a failure of one unit's electronics, actuator, or sensor does not affect the others. In contrast, because the autochambers are multiplexed to a central control box, a power or pneumatic failure at that box stops all six chambers in a stand (Fig. 6d), a known vulnerability of multiplexed systems (Görres et al. 2016). Fluxbot batteries tended to run down together because all 16 units were deployed, and later recharged, on the same day; staggering battery exchanges or solar recharging would avoid this (Forbes et al. 2023). Therefore, while multiplexed autochambers can collect data more efficiently overall, independent units such as Fluxbot 2.0 lower the risk of losing a whole array, and with it a whole site, to a single power, pneumatic, or analyzer failure, which is useful for monitoring that compares plots across landscapes or treatments.

4.5 Limitations and future directions

The comparison covered one month in autumn in one forest type at one research forest, with 10-cm soil temperatures of 11–19 °C; performance under growing-season fluxes, freezing, and snow cover remains to be tested. Neither system detected a difference between the two stands in October. Soil respiration at Harvard Forest varies widely among stands and seasons, and differences between sites can be largest in late summer and early autumn (Giasson et al. 2013; Phillips et al. 2010), so growing-season deployments are needed to test whether Fluxbot arrays resolve differences between sites. The two systems did not share collars, so system and spatial effects cannot be fully separated; rotating Fluxbots across autochamber collars would do so. Fluxbot fluxes depend on the flux model and fit window, and the sensors are vulnerable to

wetting. Future deployments should include records spanning seasons, local soil temperature and moisture at each unit, and periodic span checks. Measuring other greenhouse gases (e.g., CH_4, N_2O), integrating Fluxbot data with remote sensing and models, and improving moisture protection, power management, and maintenance are priorities for sustained distributed sensor networks.

4.6 Conclusions

Across two stands in one autumn month, arrays of low-cost, autonomous chambers matched the mean flux of a reference autochamber network within 0.3%, and their gap-filled monthly budget, averaged across stands, was about 2% lower, with differences in level no larger than expected from sampling different collars. Both systems showed late-day flux maxima and similar between-chamber variation. Hourly values agreed less closely. Fluxbot fluxes were depressed during likely sensor wetting, which the units' humidity records could flag, whereas missing records caused most data loss. At the observed variability, about 11 independent chambers per stand would give a projected 95% CI half-width of 20% of the mean. Each Fluxbot operated on its own battery and reported by cellular telemetry, allowing the two stands to be monitored without separate control stations. Low-cost chamber arrays thus relax the trade-off between temporal resolution and spatial replication and extent that has long constrained continuous soil efflux measurements. By extending continuous measurements across space, they can improve the parameterization of ecosystem models, support carbon monitoring from plots to landscapes, and clarify how ecosystems respond to environmental change.

Acknowledgements

We thank Connor Pan for system design and engineering leadership. Marc-Andre Giasson and Kathleen Savage contributed to establishing the autochamber systems. Xavier Murrell, Hector Castillo, Quentin Bateux, Brandon Lin, Ian Richardson, and Annise Dobson contributed to Fluxbot construction. Mark Van Scoy managed autochamber field operations and maintenance. Dave Orwig, Alassane Sow, Ravish Dubey, and Xuhui Lee provided essential context from prior research and ongoing monitoring efforts at Harvard Forest. Jackie Matthes and Peter Raymond offered valuable logistical support and insightful discussion. Kelly Caylor offered essential feedback on the Fluxbot 2.0 redesign. We acknowledge the Harvard Forest LTER program, Emery Boose for providing meteorological data from the Fisher Meteorological Station (HF001), and Harvard Forest staff for facilitating site access and support. This research was conducted at the Harvard Forest Long Term Ecological Research site, which was supported by the National Science Foundation LTER grant DEB-1832210.

Funding

Elizabeth Forbes was supported by an NSF Postdoctoral Research Fellowship in Biology (award number 2109902), with research support from the Yale Center for Natural Carbon Capture. Jonathan Gewirtzman was supported by an NSF Graduate Research Fellowship, the Yale Institute for Biospheric Studies, a Harvard Forest LTER Graduate Student Research Award, and a Kohlberg-Donohoe Research Fellowship from the Yale-Myers Forest. Matthew A. Nieland was supported by a USDA-NIFA Postdoctoral Fellowship (award number 2024-67012-43175). Ashley Keiser was supported by the DOE-Office of Science, Environmental Systems Science Division (award # DE-SC0025103) and the U.S. Forest Service Evaluation Monitoring Program

(award 22-DG-11094200-204). Corey Palmer was supported by the U.S. Forest Service Evaluation Monitoring Program (award 22-DG-11094200-204). The Harvard Forest LTER program is supported by the National Science Foundation (DEB-1832210).

Declaration of competing interest

The authors declare that they have no known competing financial interests or personal relationships that could have appeared to influence the work reported in this paper.

CRediT authorship contribution statement

Jonathan Gewirtzman: Conceptualization, Methodology, Software, Validation, Formal analysis, Investigation, Resources, Data curation, Writing – original draft, Writing – review & editing, Visualization, Supervision, Project administration, Funding acquisition. **Ashley Keiser:** Investigation, Resources, Data curation, Project administration, Writing – review & editing. **Matthew A. Nieland:** Methodology, Software, Validation, Investigation, Resources, Data curation, Writing – review & editing. **Corey Palmer:** Investigation, Resources, Project administration, Writing – review & editing. **Vatsal Patel:** Methodology, Resources, Project administration, Writing – review & editing. **Elizabeth Forbes:** Conceptualization, Methodology, Software, Validation, Formal analysis, Investigation, Resources, Data curation, Writing – original draft, Writing – review & editing, Visualization, Supervision, Project administration, Funding acquisition.

Data availability

Raw data, cleaned datasets, and analysis code are archived on Zenodo (Gewirtzman and Forbes 2026; https://doi.org/10.5281/zenodo.24065460) and available at

https://github.com/elizabethforbes/HarvardForest_fluxbot (tag v2.0-afm-submission). A single script (manuscript_code/run_all.R) recalculates fluxes, applies quality-control rules, and regenerates the analytical results, analysis figures, and SI tables.

Declaration of generative AI and AI-assisted technologies in the writing process

During the preparation of this work the authors used Claude (Anthropic) to assist with data analysis, code review, and editing of the text. After using this tool, the authors reviewed and edited the content as needed and take full responsibility for the content of the publication.

References

Akoglu, H., 2018. User's guide to correlation coefficients. Turkish Journal of Emergency Medicine 18, 91–93. https://doi.org/10.1016/j.tjem.2018.08.001.

Al Hamwi, W., Dubbert, M., Schaller, J., Lück, M., Schmidt, M., Hoffmann, M., 2024. Technical note: a low-cost, automatic soil–plant–atmosphere enclosure system to investigate CO2 and evapotranspiration flux dynamics. Biogeosciences 21, 5639–5651. https://doi.org/10.5194/bg-21-5639-2024.

Baldocchi, D.D., 2003. Assessing the eddy covariance technique for evaluating carbon dioxide exchange rates of ecosystems: past, present and future. Global Change Biology 9, 479–492. https://doi.org/10.1046/j.1365-2486.2003.00629.x.

Bastviken, D., Sundgren, I., Natchimuthu, S., Reyier, H., Gålfalk, M., 2015. Technical note: cost-efficient approaches to measure carbon dioxide (CO2) fluxes and concentrations in terrestrial and aquatic environments using mini loggers. Biogeosciences 12, 3849–3859. https://doi.org/10.5194/bg-12-3849-2015.

626 Bastviken, D., Wilk, J., Duc, N.T., Gålfalk, M., Karlson, M., Neset, T.-S., Opach, T., Enrich-
627 Prast, A., Sundgren, I., 2022. Critical method needs in measuring greenhouse gas fluxes.
628 Environmental Research Letters 17, 104009. https://doi.org/10.1088/1748-9326/ac8fa9.

629 Blackstock, J.M., Covington, M.D., Perne, M., Myre, J.M., 2019. Monitoring atmospheric, soil,
630 and dissolved CO2 using a low-cost, Arduino monitoring platform (CO2-LAMP): theory,
631 fabrication, and operation. Frontiers in Earth Science 7, 313.
632 https://doi.org/10.3389/feart.2019.00313.

633 Bland, J.M., Altman, D.G., 1986. Statistical methods for assessing agreement between two
634 methods of clinical measurement. The Lancet 327, 307–310. https://doi.org/10.1016/S0140-
635 6736(86)90837-8.

636 Bond-Lamberty, B., Christianson, D.S., Malhotra, A., Pennington, S.C., Sihi, D., AghaKouchak,
637 A., Anjileli, H., Arain, M.A., Armesto, J.J., Ashraf, S., et al., 2020. COSORE: a community
638 database for continuous soil respiration and other soil–atmosphere greenhouse gas flux data.
639 Global Change Biology 26, 7268–7283. https://doi.org/10.1111/gcb.15353.

640 Bond-Lamberty, B., Thomson, A., 2010. Temperature-associated increases in the global soil
641 respiration record. Nature 464, 579–582. https://doi.org/10.1038/nature08930.

642 [dataset] Boose, E., VanScoy, M., 2025. Fisher meteorological station at Harvard Forest since
643 2001. Environmental Data Initiative.
644 https://doi.org/10.6073/pasta/7a7ffd2eaa2ea9965d701998d4e2b1f5.

Bradford, J.B., Ryan, M.G., 2008. Quantifying soil respiration at landscape scales, in: Hoover, C.M. (Ed.), Field Measurements for Forest Carbon Monitoring. Springer Netherlands, Dordrecht, pp. 143–162. https://doi.org/10.1007/978-1-4020-8506-2_11.

Bradford, M.A., Oldfield, E.E., Arredondo, M.G., Black, H.I.J., Forbes, E.S., Jevon, F.V., Kelly, C., Lavallee, J.M., Liu, S., Polussa, A., et al., 2025. Agricultural soil carbon: a call for improved evidence of climate mitigation. White paper, Yale Applied Science Synthesis Program and Environmental Defense Fund. https://doi.org/10.31219/osf.io/uk3n2_v1.

Brändle, J., Kunert, N., 2019. A new automated stem CO2 efflux chamber based on industrial ultra-low-cost sensors. Tree Physiology 39, 1975–1983. https://doi.org/10.1093/treephys/tpz104.

Burba, G., 2025. Harvesting carbon: fields & grasslands. A guide to utilizing direct flux measurements for assessment and verification of carbon sequestration and GHG emission rates over areas. Preprint, ESS Open Archive. https://doi.org/10.22541/essoar.173884298.81896551/v1.

Carbone, M.S., Seyednasrollah, B., Rademacher, T.T., Basler, D., Le Moine, J.M., Beals, S., Beasley, J., Greene, A., Kelroy, J., Richardson, A.D., 2019. Flux Puppy – an open-source software application and portable system design for low-cost manual measurements of CO2 and H2O fluxes. Agricultural and Forest Meteorology 274, 1–6. https://doi.org/10.1016/j.agrformet.2019.04.012.

Carey, J.C., Tang, J., Templer, P.H., Kroeger, K.D., Crowther, T.W., Burton, A.J., Dukes, J.S., Emmett, B., Frey, S.D., Heskel, M.A., et al., 2016. Temperature response of soil respiration largely unaltered with experimental warming. Proceedings of the National Academy of Sciences of the United States of America 113, 13797–13802. https://doi.org/10.1073/pnas.1605365113.

Castell, N., Dauge, F.R., Schneider, P., Vogt, M., Lerner, U., Fishbain, B., Broday, D., Bartonova, A., 2017. Can commercial low-cost sensor platforms contribute to air quality monitoring and exposure estimates? Environment International 99, 293–302. https://doi.org/10.1016/j.envint.2016.12.007.

Cui, L., Han, W., Li, P., Fu, X., Zhai, X., Leghari, S.J., Dan, X., Xu, Q., 2026. A low-cost multi-channel automated chamber system for real-time monitoring of CO2 and H2O fluxes in maize fields. Smart Agricultural Technology 14, 102120. https://doi.org/10.1016/j.atech.2026.102120.

Curcoll, R., Morguí, J.-A., Kamnang, A., Cañas, L., Vargas, A., Grossi, C., 2022. Metrology for low-cost CO2 sensors applications: the case of a steady-state through-flow (SS-TF) chamber for CO2 fluxes observations. Atmospheric Measurement Techniques 15, 2807–2818. https://doi.org/10.5194/amt-15-2807-2022.

Davidson, E.A., Janssens, I.A., 2006. Temperature sensitivity of soil carbon decomposition and feedbacks to climate change. Nature 440, 165–173. https://doi.org/10.1038/nature04514.

Davidson, E.A., Richardson, A.D., Savage, K.E., Hollinger, D.Y., 2006. A distinct seasonal pattern of the ratio of soil respiration to total ecosystem respiration in a spruce-dominated forest. Global Change Biology 12, 230–239. https://doi.org/10.1111/j.1365-2486.2005.01062.x.

Davidson, E.A., Savage, K., Verchot, L.V., Navarro, R., 2002. Minimizing artifacts and biases in chamber-based measurements of soil respiration. Agricultural and Forest Meteorology 113, 21–37. https://doi.org/10.1016/S0168-1923(02)00100-4.

DeCarlo, K.F., Caylor, K.K., 2019. Biophysical effects on soil crack morphology in a faunally active dryland vertisol. Geoderma 334, 134–145. https://doi.org/10.1016/j.geoderma.2018.07.042.

Dubey, R., Telles, A., Nikkel, J., Cao, C., Gewirtzman, J., Raymond, P.A., Lee, X., 2024. Low-cost CO2 NDIR sensors: performance evaluation and calibration using machine learning techniques. Sensors 24, 5675. https://doi.org/10.3390/s24175675.

Ferraro, K.M., Lienau, J.R., 2025. Of all shapes and sizes: a theoretical framework for animal-mediated terrestrial heterogeneity across scales. Ecography 2025, e08006. https://doi.org/10.1002/ecog.08006.

[dataset] Finzi, A., Keiser, A., Giasson, M.-A., Nieland, M., 2026. Soil carbon in a hemlock stand infected by hemlock woolly adelgid at Harvard Forest since 2015. Harvard Forest Data Archive: HF293 (v.10). Environmental Data Initiative. https://doi.org/10.6073/pasta/a4ebf6b3eb19d832fcf09c81ec6dfa73.

Forbes, E., Benenati, V., Frey, S., Hirsch, M., Koech, G., Lewin, G., Mantas, J.N., Caylor, K., 2023. Fluxbots: a method for building, deploying, collecting and analyzing data from an array of inexpensive, autonomous soil carbon flux chambers. Journal of Geophysical Research: Biogeosciences 128, e2023JG007451. https://doi.org/10.1029/2023JG007451.

Forbes, E.S., Cushman, J.H., Burkepile, D.E., Young, T.P., Klope, M., Young, H.S., 2019. Synthesizing the effects of large, wild herbivore exclusion on ecosystem function. Functional Ecology 33, 1597–1610. https://doi.org/10.1111/1365-2435.13376.

Friedlingstein, P., O'Sullivan, M., Jones, M.W., Andrew, R.M., Hauck, J., Landschützer, P., Le Quéré, C., Li, H., Luijkx, I.T., Olsen, A., et al., 2025. Global Carbon Budget 2024. Earth System Science Data 17, 965–1039. https://doi.org/10.5194/essd-17-965-2025.

Gachibu Wangari, E., Mwangada Mwanake, R., Houska, T., Kraus, D., Gettel, G.M., Kiese, R., Breuer, L., Butterbach-Bahl, K., 2023. Identifying landscape hot and cold spots of soil greenhouse gas fluxes by combining field measurements and remote sensing data. Biogeosciences 20, 5029–5067. https://doi.org/10.5194/bg-20-5029-2023.

Gagnon, S., L'Hérault, E., Lemay, M., Allard, M., 2016. New low-cost automated system of closed chambers to measure greenhouse gas emissions from the tundra. Agricultural and Forest Meteorology 228–229, 29–41. https://doi.org/10.1016/j.agrformet.2016.06.012.

Garvey, S.M., Templer, P.H., Pierce, E.A., Reinmann, A.B., Hutyra, L.R., 2022. Diverging patterns at the forest edge: soil respiration dynamics of fragmented forests in urban and rural areas. Global Change Biology 28, 3094–3109. https://doi.org/10.1111/gcb.16099.

[dataset] Gewirtzman, J., Forbes, E., 2026. Data and code for: Low-cost autonomous chambers enable high spatial and temporal resolution monitoring of soil CO2 efflux across landscapes (version 2). Zenodo. https://doi.org/10.5281/zenodo.24065460.

Giasson, M.-A., Ellison, A.M., Bowden, R.D., Crill, P.M., Davidson, E.A., Drake, J.E., Frey, S.D., Hadley, J.L., Lavine, M., Melillo, J.M., et al., 2013. Soil respiration in a northeastern US temperate forest: a 22-year synthesis. Ecosphere 4, art140. https://doi.org/10.1890/ES13.00183.1.

Gini, C., 1912. Variabilità e mutabilità. Tipografia di Paolo Cuppini, Bologna.

Görres, C.-M., Kammann, C., Ceulemans, R., 2016. Automation of soil flux chamber measurements: potentials and pitfalls. Biogeosciences 13, 1949–1966. https://doi.org/10.5194/bg-13-1949-2016.

727 Harmon, T.C., Dierick, D., Trahan, N., Allen, M.F., Rundel, P.W., Oberbauer, S.F.,
728 Schwendenmann, L., Zelikova, T.J., 2015. Low-cost soil CO2 efflux and point concentration
729 sensing systems for terrestrial ecology applications. Methods in Ecology and Evolution 6, 1358–
730 1362. https://doi.org/10.1111/2041-210X.12426.

731 Hasenfratz, D., Saukh, O., Walser, C., Hueglin, C., Fierz, M., Arn, T., Beutel, J., Thiele, L., 2015.
732 Deriving high-resolution urban air pollution maps using mobile sensor nodes. Pervasive and
733 Mobile Computing 16, 268–285. https://doi.org/10.1016/j.pmcj.2014.11.008.

734 Hashimoto, S., Ito, A., Nishina, K., 2023. Divergent data-driven estimates of global soil
735 respiration. Communications Earth & Environment 4, 460. https://doi.org/10.1038/s43247-023-
736 01136-2.

737 Heger, A., Kleinschmidt, V., Gröngröft, A., Kutzbach, L., Eschenbach, A., 2020. Application of a
738 low-cost NDIR sensor module for continuous measurements of in situ soil CO2 concentration.
739 Journal of Plant Nutrition and Soil Science 183, 557–561. https://doi.org/10.1002/jpln.201900493.

740 Helm, J., Hartmann, H., Göbel, M., Hilman, B., Herrera Ramírez, D., Muhr, J., 2021. Low-cost
741 chamber design for simultaneous CO2 and O2 flux measurements between tree stems and the
742 atmosphere. Tree Physiology 41, 1767–1780. https://doi.org/10.1093/treephys/tpab022.

743 Hollinger, D.Y., Aber, J., Dail, B., Davidson, E.A., Goltz, S.M., Hughes, H., Leclerc, M.Y., Lee,
744 J.T., Richardson, A.D., Rodrigues, C., et al., 2004. Spatial and temporal variability in forest–
745 atmosphere CO2 exchange. Global Change Biology 10, 1689–1706.
746 https://doi.org/10.1111/j.1365-2486.2004.00847.x.

747 Huang, N., Wang, L., Song, X.-P., Black, T.A., Jassal, R.S., Myneni, R.B., Wu, C., Wang, L.,
748 Song, W., Ji, D., et al., 2020. Spatial and temporal variations in global soil respiration and their
749 relationships with climate and land cover. Science Advances 6, eabb8508.
750 https://doi.org/10.1126/sciadv.abb8508.

751 Hüppi, R., Felber, R., Krauss, M., Six, J., Leifeld, J., Fuß, R., 2018. Restricting the nonlinearity
752 parameter in soil greenhouse gas flux calculation for more reliable flux estimates. PLoS ONE 13,
753 e0200876. https://doi.org/10.1371/journal.pone.0200876.

754 Hutchinson, G.L., Mosier, A.R., 1981. Improved soil cover method for field measurement of
755 nitrous oxide fluxes. Soil Science Society of America Journal 45, 311–316.
756 https://doi.org/10.2136/sssaj1981.03615995004500020017x.

757 Jevon, F.V., Gewirtzman, J., Lang, A.K., Ayres, M.P., Matthes, J.H., 2023. Tree species effects
758 on soil CO2 and CH4 fluxes in a mixed temperate forest. Ecosystems 26, 1587–1602.
759 https://doi.org/10.1007/s10021-023-00852-2.

760 Jian, J., Steele, M.K., Thomas, R.Q., Day, S.D., Hodges, S.C., 2018. Constraining estimates of
761 global soil respiration by quantifying sources of variability. Global Change Biology 24, 4143–
762 4159. https://doi.org/10.1111/gcb.14301.

763 Keiser, A.D., Davis, C.L., Smith, M., Bell, S.L., Hobbie, E.A., Hofmockel, K.S., 2024. Depth
764 and microtopography influence microbial biogeochemical processes in a forested peatland. Plant
765 and Soil 509, 833–846. https://doi.org/10.1007/s11104-024-06895-1.

766 Kim, N., Jang, C., Yang, W.H., Guan, K., DeLucia, E.H., Lee, D., 2025. Spatial variability of
767 agricultural soil carbon dioxide and nitrous oxide fluxes: characterization and recommendations

768 from spatially high-resolution, multi-year dataset. Agriculture, Ecosystems & Environment 387,
769 109636. https://doi.org/10.1016/j.agee.2025.109636.

770 Leon, E., Vargas, R., Bullock, S., Lopez, E., Panosso, A.R., La Scala Jr., N., 2014. Hot spots, hot
771 moments, and spatio-temporal controls on soil CO2 efflux in a water-limited ecosystem. Soil
772 Biology and Biochemistry 77, 12–21. https://doi.org/10.1016/j.soilbio.2014.05.029.

773 Liang, N., Inoue, G., Fujinuma, Y., 2003. A multichannel automated chamber system for
774 continuous measurement of forest soil CO2 efflux. Tree Physiology 23, 825–832.
775 https://doi.org/10.1093/treephys/23.12.825.

776 Lin, L.I.-K., 1989. A concordance correlation coefficient to evaluate reproducibility. Biometrics
777 45, 255–268. https://doi.org/10.2307/2532051.

778 Lloyd, J., Taylor, J.A., 1994. On the temperature dependence of soil respiration. Functional
779 Ecology 8, 315–323. https://doi.org/10.2307/2389824.

780 Macagga, R., Asante, M., Sossa, G., Antonijević, D., Dubbert, M., Hoffmann, M., 2024.
781 Validation and field application of a low-cost device to measure CO2 and evapotranspiration (ET)
782 fluxes. Atmospheric Measurement Techniques 17, 1317–1332. https://doi.org/10.5194/amt-17-
783 1317-2024.

784 Martin, C.R., Zeng, N., Karion, A., Dickerson, R.R., Ren, X., Turpie, B.N., Weber, K.J., 2017.
785 Evaluation and environmental correction of ambient CO2 measurements from a low-cost NDIR
786 sensor. Atmospheric Measurement Techniques 10, 2383–2395. https://doi.org/10.5194/amt-10-
787 2383-2017.

788 Martin, J.G., Bolstad, P.V., 2009. Variation of soil respiration at three spatial scales: components
789 within measurements, intra-site variation and patterns on the landscape. Soil Biology and
790 Biochemistry 41, 530–543. https://doi.org/10.1016/j.soilbio.2008.12.012.

791 Müller, M., Graf, P., Meyer, J., Pentina, A., Brunner, D., Perez-Cruz, F., Hüglin, C.,
792 Emmenegger, L., 2020. Integration and calibration of non-dispersive infrared (NDIR) CO2 low-
793 cost sensors and their operation in a sensor network covering Switzerland. Atmospheric
794 Measurement Techniques 13, 3815–3834. https://doi.org/10.5194/amt-13-3815-2020.

795 Nguyen, T.T., Bekin, N., Altman, A., Maier, M., Agam, N., Levintal, E., 2025. Overcoming
796 barriers in long-term, continuous monitoring of soil CO2 flux: a low-cost sensor system. SOIL 11,
797 639–653. https://doi.org/10.5194/soil-11-639-2025.

798 Novick, K.A., Metzger, S., Anderegg, W.R.L., Barnes, M., Cala, D.S., Guan, K., Hemes, K.S.,
799 Hollinger, D.Y., Kumar, J., Litvak, M., et al., 2022. Informing nature-based climate solutions for
800 the United States with the best-available science. Global Change Biology 28, 3778–3794.
801 https://doi.org/10.1111/gcb.16156.

802 Ohashi, M., Kume, T., Yamane, S., Suzuki, M., 2007. Hot spots of soil respiration in an Asian
803 tropical rainforest. Geophysical Research Letters 34, 2007GL029587.
804 https://doi.org/10.1029/2007GL029587.

805 Ondier, J., Okach, D.O., John, O.C., Otieno, D.O., 2020. Influence of rainfall amount and
806 livestock grazing on soil respiration in a moist Kenyan savannah. African Journal of Ecology 58,
807 92–99. https://doi.org/10.1111/aje.12670.

Pan, C., Patel, V., Gewirtzman, J., Richardson, I., Dubey, R., Caylor, K., Dollar, A., Forbes, E., 2024. Fluxbot: the next generation – design and validation of a wireless, open-source mechatronic CO2 flux sensing chamber, in: Proceedings of the 7th ACM SIGCAS/SIGCHI Conference on Computing and Sustainable Societies. ACM, New York, pp. 85–96. https://doi.org/10.1145/3674829.3675063.

Paustian, K., Andrén, O., Janzen, H.H., Lal, R., Smith, P., Tian, G., Tiessen, H., Van Noordwijk, M., Woomer, P.L., 1997. Agricultural soils as a sink to mitigate CO2 emissions. Soil Use and Management 13, 230–244. https://doi.org/10.1111/j.1475-2743.1997.tb00594.x.

Paustian, K., Lehmann, J., Ogle, S., Reay, D., Robertson, G.P., Smith, P., 2016. Climate-smart soils. Nature 532, 49–57. https://doi.org/10.1038/nature17174.

Paustian, K., Six, J., Elliott, E.T., Hunt, H.W., 2000. Management options for reducing CO2 emissions from agricultural soils. Biogeochemistry 48, 147–163. https://doi.org/10.1023/A:1006271331703.

Pavelka, M., Acosta, M., Kiese, R., Altimir, N., Brümmer, C., Crill, P., Darenova, E., Fuß, R., Gielen, B., Graf, A., et al., 2018. Standardisation of chamber technique for CO2, N2O and CH4 fluxes measurements from terrestrial ecosystems. International Agrophysics 32, 569–587. https://doi.org/10.1515/intag-2017-0045.

Phillips, S.C., Varner, R.K., Frolking, S., Munger, J.W., Bubier, J.L., Wofsy, S.C., Crill, P.M., 2010. Interannual, seasonal, and diel variation in soil respiration relative to ecosystem respiration at a wetland to upland slope at Harvard Forest. Journal of Geophysical Research: Biogeosciences 115, G02019. https://doi.org/10.1029/2008JG000858.

Premke, K., Attermeyer, K., Augustin, J., Cabezas, A., Casper, P., Deumlich, D., Gelbrecht, J., Gerke, H.H., Gessler, A., Grossart, H.-P., et al., 2016. The importance of landscape diversity for carbon fluxes at the landscape level: small-scale heterogeneity matters. WIREs Water 3, 601–617. https://doi.org/10.1002/wat2.1147.

Pumpanen, J., Kolari, P., Ilvesniemi, H., Minkkinen, K., Vesala, T., Niinistö, S., Lohila, A., Larmola, T., Morero, M., Pihlatie, M., et al., 2004. Comparison of different chamber techniques for measuring soil CO2 efflux. Agricultural and Forest Meteorology 123, 159–176. https://doi.org/10.1016/j.agrformet.2003.12.001.

R Core Team, 2024. R: a language and environment for statistical computing. R Foundation for Statistical Computing, Vienna, Austria.

Raich, J.W., Potter, C.S., Bhagawati, D., 2002. Interannual variability in global soil respiration, 1980–94. Global Change Biology 8, 800–812. https://doi.org/10.1046/j.1365-2486.2002.00511.x.

Reinmann, A.B., Smith, I.A., Thompson, J.R., Hutyra, L.R., 2020. Urbanization and fragmentation mediate temperate forest carbon cycle response to climate. Environmental Research Letters 15, 114036. https://doi.org/10.1088/1748-9326/abbf16.

Rheault, K., Christiansen, J.R., Larsen, K.S., 2024. goFlux: a user-friendly way to calculate GHG fluxes yourself, regardless of user experience. Journal of Open Source Software 9, 6393. https://doi.org/10.21105/joss.06393.

Risch, A.C., Haynes, A.G., Busse, M.D., Filli, F., Schütz, M., 2013. The response of soil CO2 fluxes to progressively excluding vertebrate and invertebrate herbivores depends on ecosystem type. Ecosystems 16, 1192–1202. https://doi.org/10.1007/s10021-013-9676-x.

Risk, D., Nickerson, N., Creelman, C., McArthur, G., Owens, J., 2011. Forced Diffusion soil flux: a new technique for continuous monitoring of soil gas efflux. Agricultural and Forest Meteorology 151, 1622–1631. https://doi.org/10.1016/j.agrformet.2011.06.020.

Rodeghiero, M., Cescatti, A., 2008. Spatial variability and optimal sampling strategy of soil respiration. Forest Ecology and Management 255, 106–112. https://doi.org/10.1016/j.foreco.2007.08.025.

Rundel, P.W., Graham, E.A., Allen, M.F., Fisher, J.C., Harmon, T.C., 2009. Environmental sensor networks in ecological research. New Phytologist 182, 589–607. https://doi.org/10.1111/j.1469-8137.2009.02811.x.

Saunders, T., Adkins, J., Beard, K.H., Atwood, T.B., Waring, B.G., 2023. Herbivores influence biogeochemical processes by altering litter quality and quantity in a subarctic wetland. Biogeochemistry 166, 67–85. https://doi.org/10.1007/s10533-023-01098-9.

Savage, K., Davidson, E.A., Richardson, A.D., Hollinger, D.Y., 2009. Three scales of temporal resolution from automated soil respiration measurements. Agricultural and Forest Meteorology 149, 2012–2021. https://doi.org/10.1016/j.agrformet.2009.07.008.

Savage, K., Phillips, R., Davidson, E., 2014. High temporal frequency measurements of greenhouse gas emissions from soils. Biogeosciences 11, 2709–2720. https://doi.org/10.5194/bg-11-2709-2014.

Savage, K.E., Davidson, E.A., 2003. A comparison of manual and automated systems for soil CO2 flux measurements: trade-offs between spatial and temporal resolution. Journal of Experimental Botany 54, 891–899. https://doi.org/10.1093/jxb/erg121.

871 Schmitz, O.J., Wilmers, C.C., Leroux, S.J., Doughty, C.E., Atwood, T.B., Galetti, M., Davies,
872 A.B., Goetz, S.J., 2018. Animals and the zoogeochemistry of the carbon cycle. Science 362,
873 eaar3213. https://doi.org/10.1126/science.aar3213.

874 Schuirmann, D.J., 1987. A comparison of the two one-sided tests procedure and the power
875 approach for assessing the equivalence of average bioavailability. Journal of Pharmacokinetics
876 and Biopharmaceutics 15, 657–680. https://doi.org/10.1007/BF01068419.

877 Tang, J., Baldocchi, D.D., Xu, L., 2005. Tree photosynthesis modulates soil respiration on a
878 diurnal time scale. Global Change Biology 11, 1298–1304. https://doi.org/10.1111/j.1365-
879 2486.2005.00978.x.

880 Vargas, R., Carbone, M.S., Reichstein, M., Baldocchi, D.D., 2011. Frontiers and challenges in
881 soil respiration research: from measurements to model-data integration. Biogeochemistry 102, 1–
882 13. https://doi.org/10.1007/s10533-010-9462-1.

883 Wood, S.N., 2017. Generalized Additive Models: An Introduction with R, second ed. Chapman
884 and Hall/CRC, Boca Raton, FL. https://doi.org/10.1201/9781315370279.

885 Yasuda, T., Yonemura, S., Tani, A., 2012. Comparison of the characteristics of small commercial
886 NDIR CO2 sensor models and development of a portable CO2 measurement device. Sensors 12,
887 3641–3655. https://doi.org/10.3390/s120303641.

888 Zeng, X., Chen, X., Heng, L., Oshunsanya, S.O., Yu, H., 2026. Application of a high-
889 performance, low-cost portable NDIR sensor monitoring system for continuous measurements of
890 in situ soil CO2 fluxes. Sensors 26, 761. https://doi.org/10.3390/s26030761.

Supplementary material

Low-cost autonomous chambers enable high spatial and temporal resolution monitoring of soil CO_2 efflux across landscapes

Jonathan Gewirtzman, Ashley Keiser, Matthew A. Nieland, Corey Palmer, Vatsal Patel, Elizabeth Forbes

Contents

S1. Site and instruments **1**
S2. Flux calculation and quality control **2**
S2.1 Processing 2
S2.2 Fluxbot fit window 3
S2.3 Flux model 4
S2.4 Sampling rate 6
S2.5 Quality control and measurement accounting 6
S3. Agreement between systems **7**
S3.1 Statistical details 7
S3.2 Results 9
S4. Moisture and the K30 sensors **12**
S4.1 Laboratory tests 12
S4.2 Wet sensors and stuck lids in the field 15
S4.3 Data loss and bias from moisture 16
S5. Temperature response and resilience **17**
S5.1 Diel cycle and temperature response 17
S5.2 Resilience 18
References **19**

The main analysis uses fluxes from goFlux model selection (linear or Hutchinson–Mosier for each closure) for both systems, and the **RH-screened** dataset: closures that passed quality control (Section S2.5), minus Fluxbot closures with mean in-chamber RH ≥ 99% over 54:00–55:00, the open-lid minute before closure, when the K30 or its envelope is likely to be wet (Pan et al. 2024). The **as-deployed** dataset keeps the wet-sensor closures (Section S4.3). Arrays, system means, compared hours, and the offset are defined in main text Table 2. The study period was 2–31 October 2023.

S1. Site and instruments

Besides the IRGA (LI-840 at the hemlock tower and LI-800 at Bigelow Brook; LI-COR, Lincoln, NE, USA), each autochamber control box contains a pump (Brailsford TD-3LS, 12 V DC), a CR1000 datalogger, an SDM-CD16AC relay controller, a 12 V DC power supply, and the solenoid valves. Collar heights above the soil were 3.6–5.9 cm.

Each Fluxbot 2.0 has a Senseair K30 NDIR sensor (0–10,000 ppm) in a PTFE envelope, a Sensirion SHT-30 temperature and humidity sensor under a reflective radiation shield, an LPS22 pressure sensor, a servo-actuated hinged lid on a PVC sewer cap, a Voltaic Systems V50 battery pack, and a Particle Boron microcontroller that transmits data hourly over LTE. Units were placed to span the microtopography and vegetation of each stand (Fig. S1). Pan et al. (2024) describe the system in full.

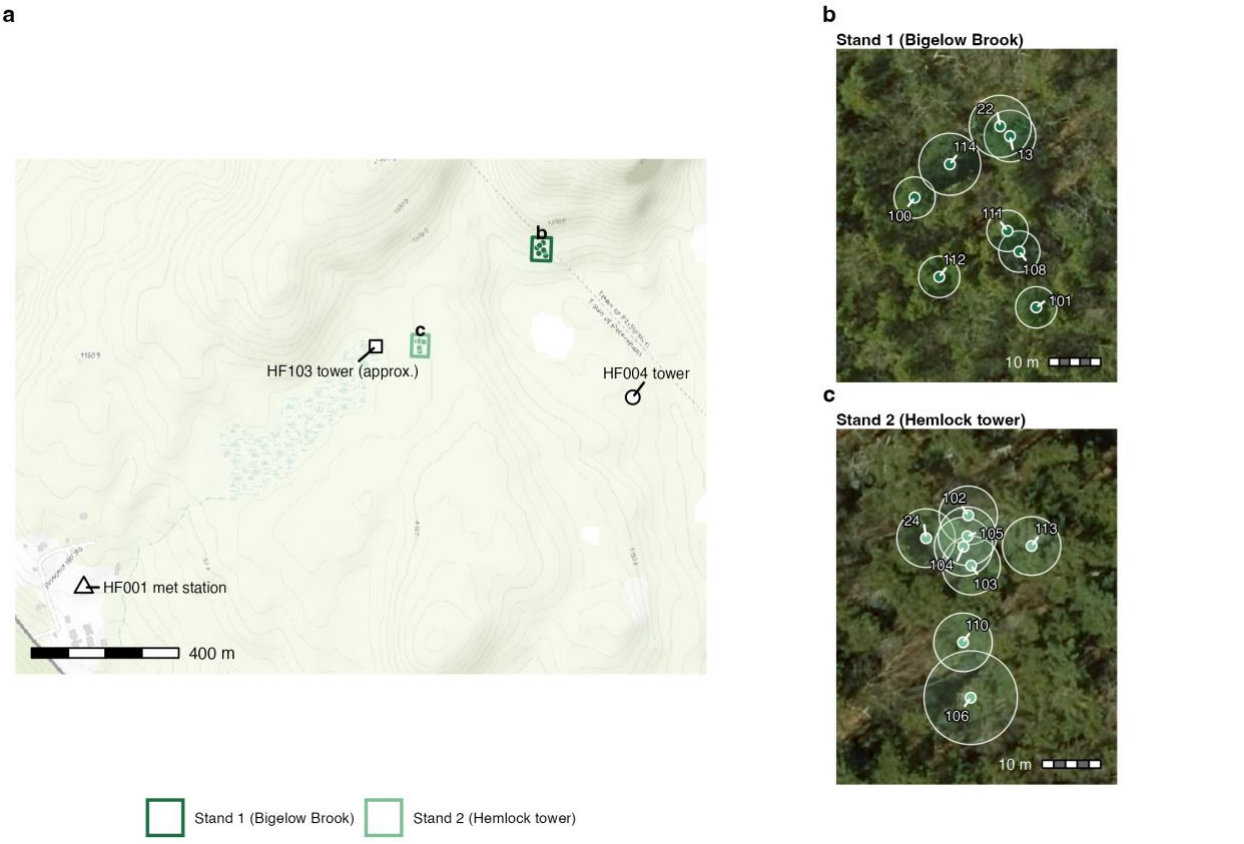


Fig. S1. *Study site. (a) The two hemlock stands, with Fluxbot units as points and boxes marking the extents of b and c, the Fisher meteorological station (HF001), and the two nearest eddy-covariance towers (HF004 and HF103); the HF103 tower position is archived to 0.001° (about ±100 m). (b, c) Fluxbot 2.0 units in each stand, from GPS positions taken on 17 November 2023; circles show each position's reported horizontal accuracy (4–8 m), so apparent overlaps between units are within GPS error. Autochamber positions were not surveyed; the autochamber arrays are in the same stands. Basemaps: (a) Tiles © Esri – Esri, DeLorme, NAVTEQ, TomTom, Intermap, iPC, USGS, FAO, NPS, NRCAN, GeoBase, Kadaster NL, Ordnance Survey, Esri Japan, METI, Esri China (Hong Kong), and the GIS User Community; (b, c) Tiles © Esri – Source: Esri, i-cubed, USDA, USGS, AEX, GeoEye, Getmapping, Aerogrid, IGN, IGP, UPR-EGP, and the GIS User Community.*

S2. Flux calculation and quality control

S2.1 Processing

We computed fluxes for both systems from the raw records with goFlux 0.4.0 (Rheault et al. 2024), with the same settings. We removed Fluxbot rows with error codes (CO_2 = 65,535 or 65,533) and set failed

SHT-30 reads (44,755.7 °C; 25,600.4 %RH) to missing. Autochamber records came from the logger's 1-Hz output; the logger and HF001 clocks are in Eastern Standard Time and were converted to local time (Eastern Daylight Time).

The main Fluxbot fit used 57:00–60:00 (Section S2.2) and required at least 15 observations spanning at least 135 s. Autochamber fits used 75–295 s after the start of each 5-min slot, after the open-lid flush, and required at least 120 observations. Pressure was station pressure, the hourly median of the Fluxbot LPS22 sensors in each stand. We excluded units whose median deviation from the hourly stand median exceeded 5 hPa in absolute value (unit 100 read 22 hPa low throughout), then recalculated the hourly stand medians; where no LPS22 data were available, HF001 pressure × 0.9597 (the median local/HF001 ratio) was used. Temperature was in-chamber air temperature for Fluxbots and HF001 air temperature for autochambers. No water-vapor correction was applied. goFlux computes minimum detectable fluxes from instrument precision, which was estimated from each system's records as 2.6 ppm for Fluxbots and 2.3 ppm for autochambers.

S2.2 Fluxbot fit window

The lid closes at 55:00, but CO_2 reaches the K30 by diffusion through its PTFE envelope. A breakpoint fit placed the start of the rise a median of 48 s after closure; the rise started after 56:00 in 35% of closures and after 57:00 in 5% (Fig. S2b). A 56:00 window gives linear fluxes 16% higher than a 57:00 window when the rise starts early and the curve is already flattening, but 6–15% lower when the rise starts after 56:00 and the window includes flat records (Fig. S2c; median ratio 1.04). With the 56:00 window, the offset was +2.9% (hourly r = 0.80; daily r = 0.85); with the 57:00 window, it was −0.3% (0.72; 0.85) (Fig. S2d). We used the 57:00–60:00 window because it starts after the diffusion delay in 95% of closures.

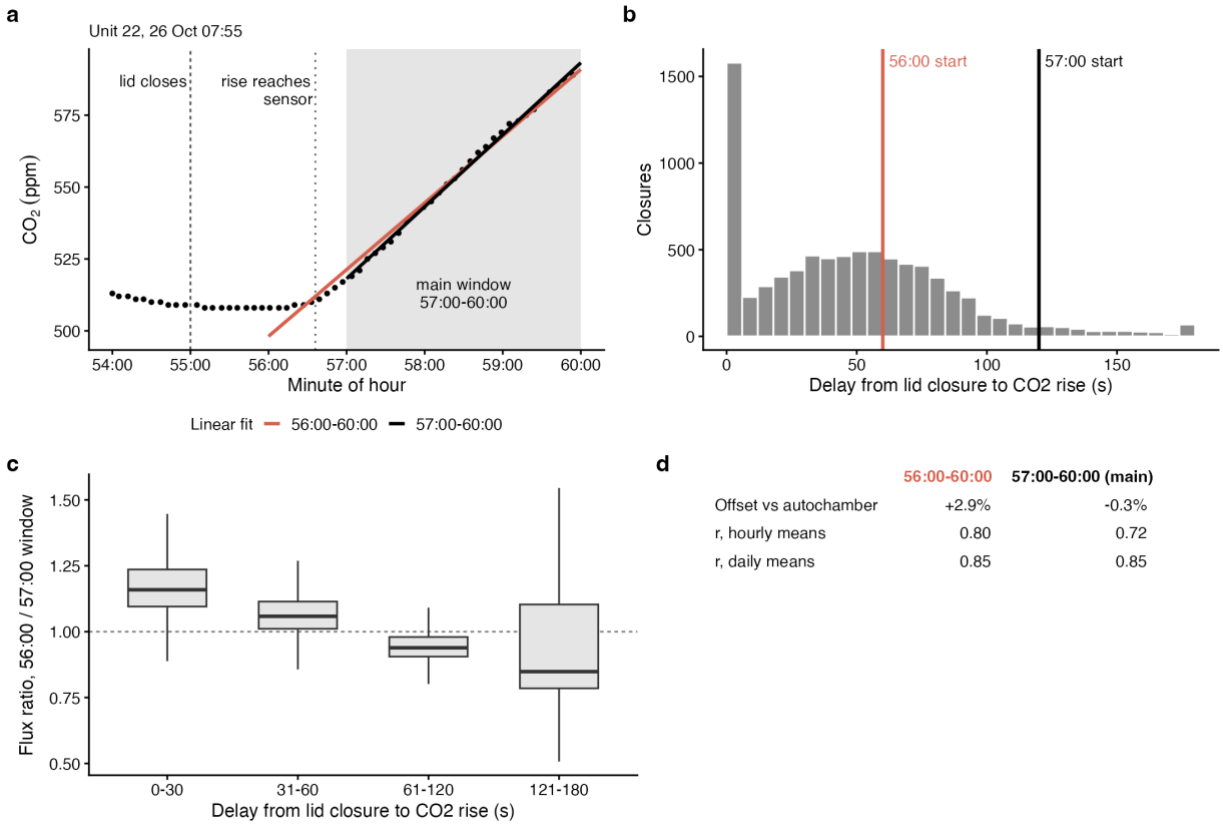


Fig. S2. *Fluxbot fit window. (a) An example closure in which the CO_2 rise reached the sensor 96 s after the lid closed, with linear fits over the 56:00–60:00 and 57:00–60:00 windows; the earlier window includes pre-rise records and underestimates the slope (shaded: main window). (b) Distribution of the delay from lid closure to the start of the rise; a delay of 0 s includes closures in which no delay could be resolved. (c) Ratio of closure fluxes from the two windows, by delay (boxes: quartiles; whiskers: 1.5 × IQR). (d) Agreement of Fluxbot and autochamber system means under each window (main dataset).*

S2.3 Flux model

For each closure, goFlux fits a linear model (LM) and the Hutchinson–Mosier model (HM; Hutchinson and Mosier 1981), and selects HM only when it meets explicit criteria, including limits on the curvature parameter κ and on the ratio of the HM to the LM flux (g-factor ≤ 2; Hüppi et al. 2018). goFlux chose HM for 90% of Fluxbot and 80% of autochamber closures, and the median ratio of model-selected to LM flux was 1.16 for Fluxbots and 1.02 for autochambers (Fig. S3a), as expected in a small headspace in which accumulating CO_2 weakens the diffusion gradient from the soil. The flux model therefore set the offset between systems (Fig. S3b): −0.3% with model selection for both systems, −11% with LM for both, and −21% to +17% for mixed pairings. With LM for both, the monthly budget ratio was 0.87 (0.74–1.04), against 0.98 (0.81–1.18) with model selection (Fig. S3c), but hourly means were more closely correlated (r = 0.81 against 0.72; difference 0.10, 95% CI 0.02–0.16 from a moving-block bootstrap with blocks of 24 consecutive matched observations). Larger HM fit errors are a possible contributor: within each system,

hourly series from the two models correlated at r = 0.97, but the standard errors of HM fits were 2.5–4 times those of LM fits. Because LM fits underestimate the flux when the concentration curve bends, we used model selection for the main analysis.

Fluxbot curvature was about three times stronger in the evening and at night (16:00–05:00) than at midday (09:00–12:00; median κ 0.0026 against 0.0009), so the model-selected flux exceeded the linear flux by a median of 21% at night but 4% at midday; autochambers showed the same pattern, but much more weakly. Curvature increased with the CO_2 concentration at the start of the fit (Spearman ρ = 0.30 for Fluxbots), which was higher at night, consistent with CO_2 accumulating near the soil surface on calm nights so that the small, unpumped Fluxbot headspace approaches saturation sooner. If so, the curvature reflects suppression of the flux by the chamber, which the HM fit is designed to correct. The autochambers support this: with linear fits, Fluxbot fluxes were 6% lower than autochamber fluxes during the day (09:00–15:00; ratio 0.94, 95% CI 0.89–0.99) but 13% lower in the evening and at night (0.87, 0.81–0.93), whereas with model selection the ratio was close to 1 in both (1.03, 0.94–1.11, and 0.98, 0.90–1.08).

Because model selection extrapolates with this curvature, it raised evening and night Fluxbot fluxes more than midday fluxes, and its larger uncertainty made the hour-of-day means noisier. With linear fits, the Fluxbot diel cycle peaked at 17:00; with model selection, it peaked at 21:00, and its hour-of-day means deviated more from a 3-h running mean (0.12 against 0.05 µmol m^{-2} s^{-1}; autochambers 0.03 and 0.02). The timing of the Fluxbot diel cycle and the Fluxbot Q_{10} (Section S5.1) are therefore sensitive to the flux model.

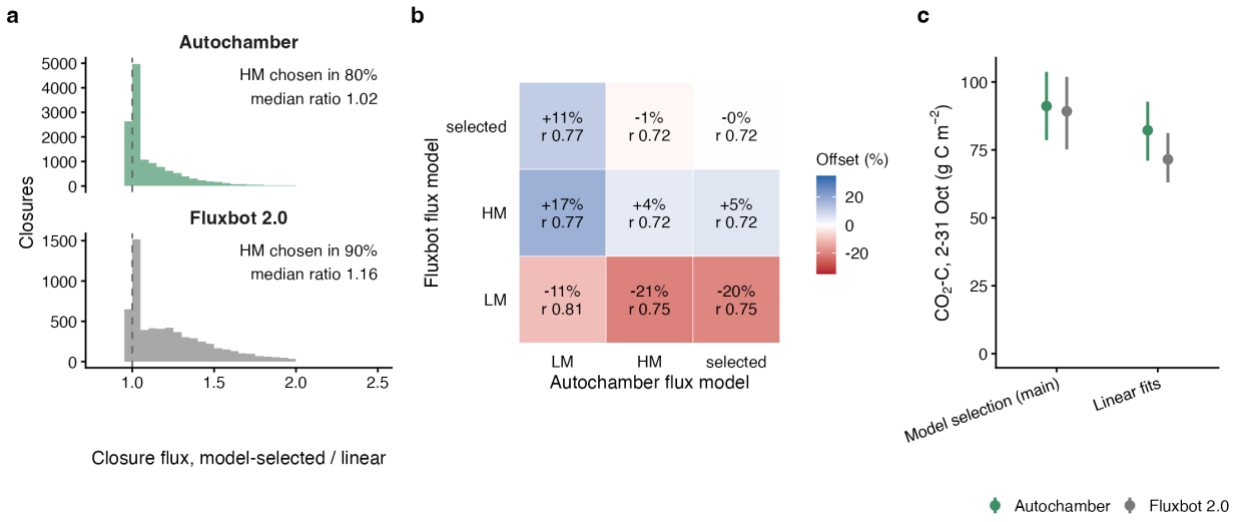


Fig. S3. *Flux model. (a) Closure-level ratio of the goFlux model-selected to the linear flux for each system. (b) Offset and hourly r for each pairing of flux models (main dataset). (c) Gap-filled monthly budgets under model selection (main) and linear fits, with chamber-bootstrap 95% CIs. Autochamber fluxes published in the Harvard Forest Data Archive (HF293; Finzi et al. 2026) are calculated with a different procedure (the best-fitting 1-min window of each*

closure, with fixed pressure and temperature) and average about a third higher than the linear fits used here; we recalculated both systems with one procedure so that differences between systems do not reflect differences in processing.

S2.4 Sampling rate

Fluxbots record about every 6 s and autochambers at 1 Hz. To test whether this difference affected the comparison, we thinned the 1-Hz autochamber records to one reading every 6 s, from a random starting offset, and recomputed each flux with the same goFlux call. The closure-level comparison included 13,755 matched fits with original linear flux above 0.3 μmol m^{-2} s^{-1}. Linear fluxes changed by a median of 0.0% (coefficient of variation, CV, 0.8% across closures) and model-selected fluxes by 0.1%, the share of closures fitted with HM was unchanged (79.4%), and hourly system means correlated with the 1-Hz means at r = 0.99999. The standard error of the slope rose 2.5-fold, but the minimum detectable flux was unchanged (ratio 1.01). The lower Fluxbot sampling rate therefore did not contribute to the differences between systems.

S2.5 Quality control and measurement accounting

A closure was counted as a chamber failure if (1) it had too few records to fit a flux (thresholds in Section S2.1); (2) the lid was stuck shut, so that the chamber did not vent between closures (below; for autochambers, CO_2 at the start of a closure more than 500 ppm above the median of the other chambers in the stand in the same hour); (3) CO_2 did not accumulate significantly (goFlux slope flag); or (4) CO_2 declined, with a significant negative linear slope. At October fluxes of about 2 μmol m^{-2} s^{-1}, a sealed chamber always accumulates CO_2, so (3) and (4) indicate a chamber that did not seal. These checks use the linear-fit diagnostics for every flux model. In addition, because the six autochambers of an array share one pump, pneumatic system, and power supply, every chamber stops sealing at once when these fail. We therefore excluded an autochamber array-hour when at least three distinct chambers had a declining slope, a nonsignificant slope, or a linear-fit R^2 below 0.5 during that assigned hour. This removed 870 closures (6.1% of computed autochamber closures), mostly on 5 and 25–30 October in stand 1. We did not apply a goodness-of-fit threshold to individual closures, because such thresholds preferentially remove small fluxes.

We identified stuck lids from the open-lid baseline anomaly: each unit's open-lid CO_2 (median over 54:00–55:00) minus the median of the other units in its stand in the same hour. We formed saturated episodes from runs of hours with in-chamber RH ≥ 99%, bridging gaps of up to 3 h, and classified a saturated episode as a stuck lid when its median open-lid CO_2 anomaly exceeded 500 ppm, meaning that the headspace was not venting between closures (Section S4.2).

Among closures that passed these checks, a per-chamber robust screen (median ± 5 median absolute deviations) removed isolated spikes, which we attribute to sensor artifacts (20 Fluxbot and 79 autochamber closures). We removed no other values and applied no value-based trimming to the pooled data. After applying the linear-fit QC rules, we retained selected fluxes with their sign, including values below the minimum detectable flux, which goFlux computes from the instrument precision: 0.6% of Fluxbot and 0.1% of autochamber fluxes in the main dataset.

For the measurement accounting (main text Fig. 6a), intended closures were one per Fluxbot and two per autochamber per hour for every installed unit over 2–31 October; units that stopped before 31 October counted as downtime.

S3. Agreement between systems

S3.1 Statistical details

Agreement of hourly and daily system means was quantified with the Pearson correlation r; Lin's concordance correlation coefficient (CCC; Lin 1989; Akoglu 2018), which combines correlation with agreement in level (1 = perfect agreement); the mean difference between systems (offset; Fluxbot minus autochamber); and the root-mean-square difference as a percentage of the mean autochamber flux (nRMSE).

We assigned each closure to the nearest clock hour using the start of its fit window, then averaged autochamber fluxes within chamber and assigned hour. Chamber-hour analyses used HF001 observations averaged within 60 min on either side of the assigned hour. The budget models used clock-hour means of soil temperature. Raising the minimum number of chambers per system and stand for a compared hour from 1 to 6 reduced the compared hours from 340 to 103, while the offset stayed between −1.6% and +1.9% and hourly r between 0.65 and 0.73. The results were therefore insensitive to this threshold; we used three, which averages over several collars in each stand while keeping most compared hours (305).

The GAM (mgcv; REML) had the form flux ~ stand + system + s(hour, cyclic) + s(10-cm soil temperature) + s(chamber, random effect). Equivalence was tested with two one-sided tests (TOST; Schuirmann 1987) on the GAM system effect and its standard error, with margins expressed as a percentage of the mean across all screened autochamber chamber-hours (2.91 μmol m^{-2} s^{-1}). For Table S2a, we calculated paired 3-h rolling means on a complete hourly grid, retained complete windows, and resampled their differences in circular blocks of 24 retained values (2,000 resamples); a block can therefore span a gap. Agreement across averaging scales (Fig. S5) was computed for non-overlapping blocks of 1, 3, 6, 12, 24, and 72 h,

unlike the 3-h rolling means of Tables S1 and S2a; a block required at least half of its hours to be compared hours.

Because the two systems measured different collars, part of any difference between them could come from the collars rather than the instruments. To test this, we compared the disagreement between systems with the disagreement between two sets of collars measured by the same system. In this spatial-null benchmark, each of 200 distinct pairings per comparison took two disjoint sets of three chambers per stand, from the same system or from different systems, and each set's mean required at least two of its three chambers in each stand. The 200 pairings are all possible pairings of autochamber sets and a random sample, without repeats, of the many more possible Fluxbot and cross-system pairings. Pairings share chambers, so they describe the range of possible collar groupings rather than independent replicates; the offset for each pairing is the mean difference over all hours both sets reported. P is the probability that a cross-system pairing disagrees more than a within-system pairing (0.5 = indistinguishable).

Monthly budgets were computed for each stand and system by gap-filling hourly stand means (at least three chambers) with a GAM of flux on 10-cm soil temperature ($k = 6$) and a cyclic smooth of hour ($k = 8$), and summing over 2–31 October. The GAM reproduced the observed stand means closely (Fig. S4). The 95% intervals, including that of the Fluxbot/autochamber ratio, came from resampling chambers within stands (200 resamples per system; the cumulative bands in main text Fig. 2c use 100). To test whether the hours with Fluxbot data were representative, we also computed a second autochamber budget from only the stand-hours in which the Fluxbot array had a stand mean, gap-filling the remaining hours in the same way (Section S4.3).

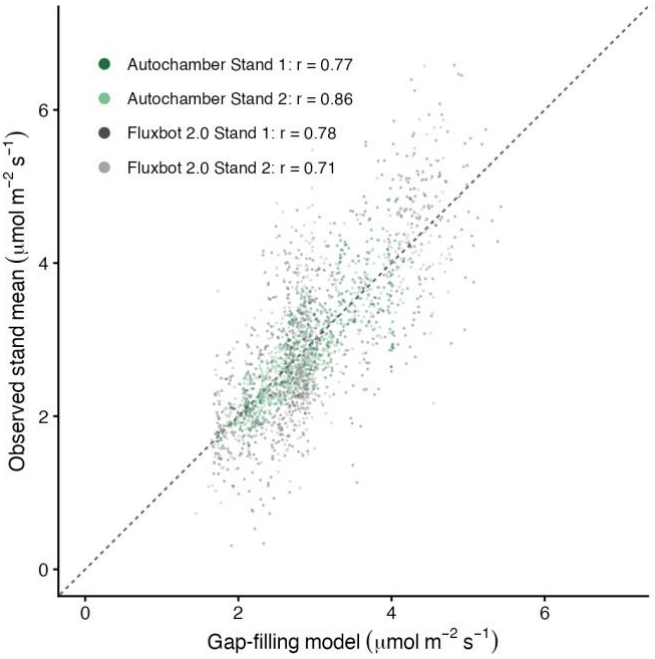


Fig. S4. *The gap-filling model: observed hourly stand means against the GAM of flux on 10-cm soil temperature and hour of day used to fill gaps in the monthly budgets, for each array (main dataset), with the correlation for each array.*

The number of chambers needed for the 95% CI of a stand mean to fall within a relative error of ±E of the mean was $n = (t_{0.975,\,n-1}\ CV/E)^2$, solved iteratively, using the CV of chamber means.

S3.2 Results

Agreement improved with longer averaging, from r = 0.72 and nRMSE = 23% for hourly system means to 0.85 and 17% for daily means, while the offset stayed within ±1% (Table S1; Fig. S5). Four 72-h blocks met the coverage criterion for the full arrays (r = 0.90). At this scale, 150 autochamber pairings, 20 Fluxbot pairings, and one cross-system pairing qualified. Disjoint three-chamber subsets of the same system agreed more closely with each other than subsets of different systems, especially at the hourly scale (median r for hourly and daily means: 0.90 and 0.95 for two autochamber subsets, 0.83 and 0.96 for two Fluxbot subsets, and 0.65 and 0.83 across systems). In the spatial-null benchmark (Section S3.1), the median absolute offset was no larger across systems (9% of the mean flux) than within autochambers (11%) or within Fluxbots (11%; P = 0.42; main text Fig. 3c), but the median hourly r was lower (0.66 across systems, against 0.90 within autochambers and 0.84 within Fluxbots; P = 0.98), as was the daily r (0.85, against 0.95 and 0.96; P = 0.86). The level difference between systems was therefore within the range expected from sampling different collars, whereas the difference in short-term dynamics was not.

Table S1. Agreement metrics for hourly, 3-h rolling, and daily system means, for the main (RH-screened) and as-deployed datasets. Offset = Fluxbot − autochamber (μmol m^{-2} s^{-1}); limits of agreement are Bland–

Altman 95% limits; OLS slope, ordinary least-squares slope of Fluxbot on autochamber means; Cb, the bias-correction factor of the CCC (1 = no difference in mean or variance).

Dataset	Scale	n	Mean, autochamber	Mean, Fluxbot	r	OLS slope	Offset	Offset (%)	RMSE	nRMSE (%)	Limits of agreement	CCC	Cb
RH-screened (main)	hourly	305	2.88	2.87	0.72	1.04	-0.01	-0.3	0.68	23.5	-1.33 to 1.32	0.67	0.94
RH-screened (main)	3-h rolling	278	2.86	2.86	0.74	1.14	0	-0.1	0.61	21.5	-1.21 to 1.20	0.68	0.92
RH-screened (main)	daily	15	2.85	2.84	0.85	1.46	-0.01	-0.3	0.47	16.6	-0.97 to 0.95	0.74	0.87
As deployed	hourly	357	2.9	2.82	0.69	0.98	-0.09	-3	0.66	22.8	-1.37 to 1.20	0.65	0.94
As deployed	3-h rolling	329	2.89	2.81	0.71	1.04	-0.08	-2.8	0.6	20.6	-1.24 to 1.08	0.66	0.92
As deployed	daily	16	2.86	2.79	0.8	1.31	-0.07	-2.6	0.46	16.1	-1.00 to 0.85	0.7	0.88

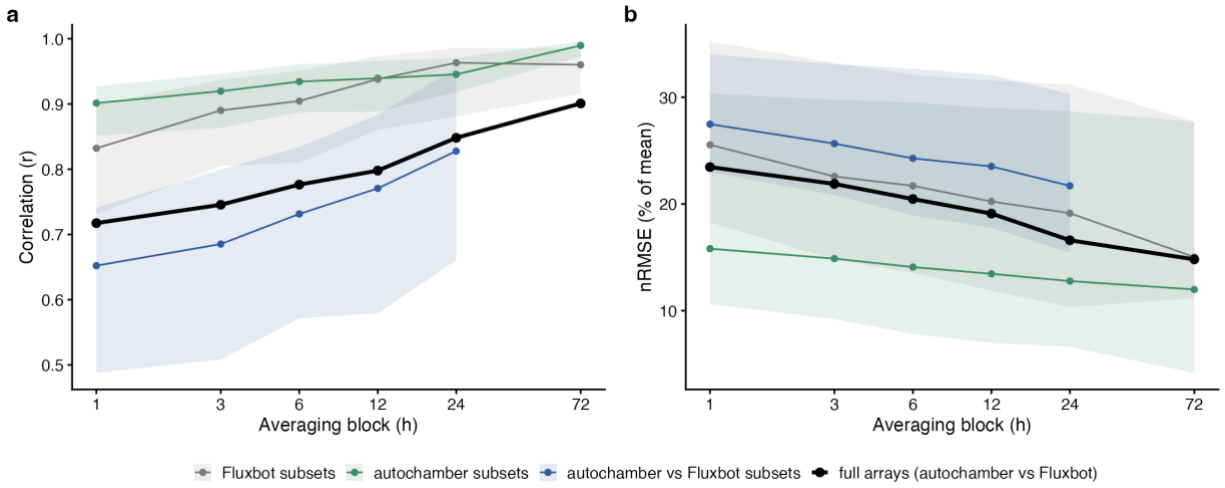


Fig. S5. *Agreement between systems compared with agreement between disjoint three-chamber subsets of the same system (autochamber–autochamber, Fluxbot–Fluxbot) and of different systems. (a) Correlation and (b) nRMSE as a function of averaging block length for the full arrays (black) and for subsets (lines: medians; bands: 10th–90th percentiles of up to 150 qualifying draws per comparison). Blocks are non-overlapping, unlike the 3-h rolling means of Tables S1 and S2a. At 72 h only one cross-system draw qualified, so no cross-system subset summary is shown.*

The GAM explained 54% of the deviance, and the hour-of-day and soil-temperature smooths were both significant ($p < 0.001$). After accounting for time of day, temperature, and differences among collars, Fluxbots read 0.05 µmol m^{-2} s^{-1} (2%) lower than autochambers (SE 0.31; 95% CI −0.66 to 0.56), a

difference that was not significant. In the equivalence test (TOST; Schuirmann 1987; main text Section 2.8), the 90% CI of this difference (−0.56 to +0.47 μmol m^{-2} s^{-1}) lay within ±19.2% of the mean across all screened autochamber chamber-hours, so differences larger than 19.2% could be excluded (p = 0.043 at ±20%) but differences of 10% could not (p = 0.22). The interval is wide mainly because collars differ from one another (between-chamber SD of 0.82 μmol m^{-2} s^{-1}, estimated by the GAM across the chambers of both systems; about 30% of the mean), which limits how closely any two sets of six to eight separate collars can be shown to agree, whatever the instruments. A linear mixed model without smooths, with random intercepts for chamber and for hour, gave nearly the same system effect (−0.05 μmol m^{-2} s^{-1}, −2%; SE 0.31), so the estimate does not depend on the smooths.

Table S2 shows how the main results depend on processing and quality-control choices (a) and on the Fluxbot data-cleaning steps (b); the flux model had the largest effect on the level (Section S2.3).

Table S2. Sensitivity of the main results. (a) Processing and quality-control choices: method effect from the GAM; offset, r, and CCC for paired 3-h rolling system means (block-bootstrap CI, Section S3.1); Q_{10} from pooled exponential fits. (b) Fluxbot data-cleaning steps (main text Fig. 6a), from stuck lids and wet sensors kept to the main dataset with additional hours removed after each wet episode: agreement of system means over compared hours.

Scenario	Fluxbot closures	Method effect (GAM, μmol m^{-2} s^{-1}; 95% CI)	Offset, 3-h system means (μmol m^{-2} s^{-1}; block-bootstrap 95% CI)	r (3-h system means)	CCC (3-h system means)	Q_{10} autochamber	Q_{10} Fluxbot
Main: RH-screened, model selection	6301	-0.05 (-0.66 to 0.56)	-0.00 (-0.22 to 0.26)	0.74	0.68	2.84	3.7
As deployed: wet-sensor closures kept	6962	-0.11 (-0.72 to 0.49)	-0.08 (-0.30 to 0.17)	0.71	0.66	2.73	3.38
Flux model: linear (LM) for all closures	6307	-0.33 (-0.83 to 0.16)	-0.27 (-0.39 to -0.14)	0.84	0.74	2.98	3.52
Flux model: Hutchinson-Mosier (HM) for all closures	6287	0.08 (-0.53 to 0.69)	0.13 (-0.09 to 0.41)	0.75	0.68	2.83	3.38
Linear fits, as deployed	6979	-0.37 (-0.87 to 0.12)	-0.33 (-0.46 to -0.19)	0.78	0.66	2.83	3.2
QC: negatives removed, then pooled 1.5 × IQR screen	7435	-0.04 (-0.58 to 0.49)	0.03 (-0.28 to 0.33)	0.34	0.33	2.34	3.58
QC: negatives removed only	7524	-0.11 (-0.71 to 0.49)	0.01 (-0.28 to 0.33)	0.45	0.43	2.97	3.88

Scenario	Fluxbot closures	Method effect (GAM, µmol m^{-2} s^{-1}; 95% CI)	Offset, 3-h system means (µmol m^{-2} s^{-1}; block-bootstrap 95% CI)	r (3-h system means)	CCC (3-h system means)	Q_{10} autochamber	Q_{10} Fluxbot
Pressure: HF001 sea-level-reduced	6301	-0.05 (-0.68 to 0.59)	-0.00 (-0.24 to 0.26)	0.74	0.68	2.84	3.7

Fluxbot data	Fluxbot closures	Compared hours	Offset (%)	r (hourly)	r (daily)
stuck lids and wet sensors kept	7420	376	-7.1	0.71	0.86
as deployed	6962	357	-3	0.69	0.8
RH-screened (main)	6301	305	-0.3	0.72	0.85
RH-screened + 1 h after wet removed	6222	301	-0.3	0.72	0.85
RH-screened + 6 h after wet removed	5878	278	0.2	0.7	0.83
RH-screened + 24 h after wet removed	5155	229	4.1	0.72	0.9

S4. Moisture and the K30 sensors

Pan et al. (2024) identified condensation on the K30 as the main cause of Fluxbot data loss and bias. Water could affect a reading in three ways, each with its own signature: (1) liquid water on the envelope could act as a diffusion barrier, slowing and damping the response so that closure slopes and fluxes are underestimated; (2) water vapor inside the sensor could affect the infrared measurement, so that the reading tracks humidity at constant CO_2, giving an offset and an apparent gain error when CO_2 and humidity change together; and (3) liquid water reaching the electronics would cause error codes, dropouts, spikes, or a sensor that stops recording. We tested these in two laboratory experiments (Section S4.1) and then examined wet sensors in the field (Sections S4.2–S4.3).

S4.1 Laboratory tests

In the first test (22 September 2023), one PTFE-covered and one uncovered K30 ran beside a laser-based reference analyzer (LGR; M-GGA-918, ABB–Los Gatos Research; 1 Hz) in a growth chamber (about 90% RH; 900 ppm CO_2); after four hours dry, the covered sensor was sprayed until water beaded on the PTFE (Fig. S6a). In the second test (13 December 2023), two covered (t1, t2) and three uncovered K30s (c1–c3) ran beside the LGR on a CO_2 rig through five phases: dry and wet PTFE envelope, dry and wet 3D-printed bracket (which held the membrane taut; not used in the field), and bare sensors sprayed (Fig. S6b). In both tests, CO_2 was varied with breath pulses and door openings.

We calibrated each K30 against the LGR on its own dry period with a lagged first-order response model, $K30(t) = a + b \cdot LGR_\tau(t - L)$, where LGR_τ is the LGR record passed through a first-order response with

time constant τ, b the gain, and L a clock lag, and compared wet periods with that calibration (offset, scatter, refitted τ and gain, error codes). Damping was measured as the covered/uncovered slope ratio on matched 90-s windows in which the LGR changed steadily (> 1 ppm s^{-1}, $R^2 > 0.9$), and vapor sensitivity by regressing the uncovered sensors' residuals on LGR H_2O. Sensor c2 was noisy throughout and was left out of the uncovered reference.

When dry, every K30 except c2 tracked the LGR linearly from about 420 to 1,700 ppm (gain 0.97–1.00, median $R^2 \geq 0.99$), reading 33–52 ppm above it, an offset that does not affect a closure slope.

Evidence for a diffusion barrier was weak (Fig. S6c). The covered/uncovered slope ratio was 0.93 dry, 0.85 with the envelope wet, and 0.98–0.99 with the bracket dry or wet. Wetting did not slow the December sensors (τ 15–20 s throughout). The dry September envelope slowed the response (τ 50 s against 30 s uncovered), close to the median 48-s delay before CO_2 rises in field closures (Section S2.2). Water vapor had a small effect (+2.4 and +2.6 ppm per ppt H_2O in c1 and c3), which over a field closure would be under about 5% of a typical slope and opposite in sign to the field wet-sensor bias.

Liquid water on the cover made readings erratic and, in some sensors, offset them upward (Fig. S6d). The scatter of the September PTFE-covered sensor rose from 11 ppm dry to 58 ppm wet, and it and the December sensor t2 read about 30 ppm above their dry calibrations. Only bare sensors failed outright: when sprayed, t1 stopped recording, t2 logged 98% error codes, and c2 read about 110 ppm high; with covers on, no sensor stopped. The tests reproduced the direction of the field behavior but not its size: field wetting lasts hours to days, through condensation as well as rain, with temperature and humidity gradients that brief sprays cannot reproduce.

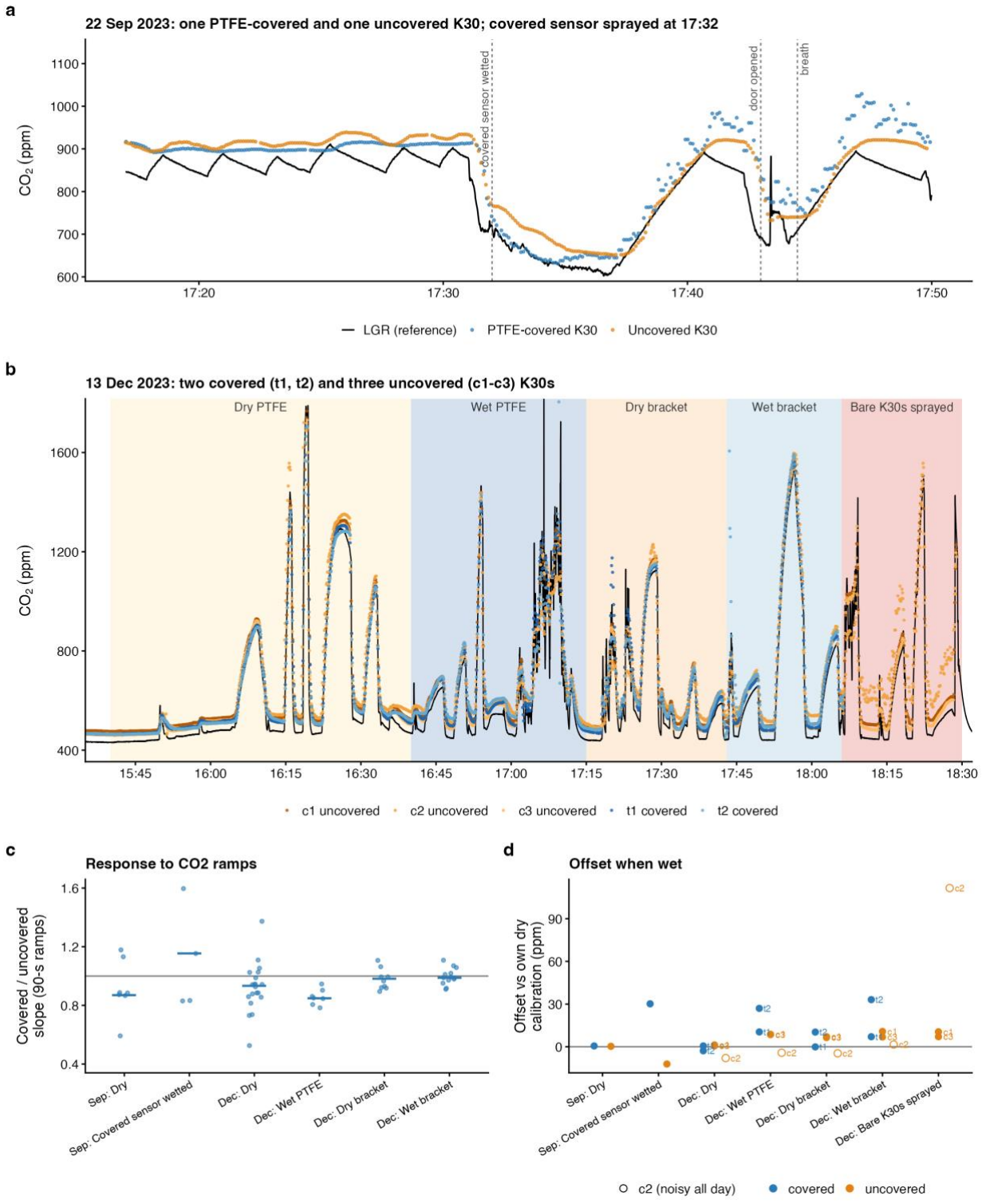


Fig. S6. *Laboratory tests of wet K30 sensors against an LGR reference (black). (a) 22 September 2023: PTFE-covered (blue) and uncovered (orange) K30, before and after the covered sensor was sprayed (17:32). (b) 13 December 2023: two covered (t1, t2) and three uncovered (c1–c3) K30s through five phases. (c) Covered/uncovered slope ratio on matched 90-s CO_2 ramps (points: ramps; bars: medians); a diffusion barrier would lower this ratio. (d) Offset of each sensor relative to its own dry calibration; open circle: c2, noisy throughout.*

S4.2 Wet sensors and stuck lids in the field

Following Pan et al. (2024), we flagged closures as wet when in-chamber RH was ≥ 99% in the open-lid minute before the lid closed. The open-lid baseline anomaly (Section S2.5) provides an independent diagnostic: a healthy sensor reads close to the other units in its stand, with a median anomaly of −3 ppm and a 90th percentile of 23 ppm in dry periods. Wet hours made up 19% of recorded unit-hours (1,678 h), occurred in all 16 units, and formed 82 episodes (runs of wet hours, bridging gaps of up to 3 h).

Seventeen episodes in 6 units (737 h), including all six longer than 48 h, were stuck lids: the open-lid CO_2 anomaly exceeded 500 ppm as a median over the episode, reaching several thousand ppm, so the headspace was not venting between closures. Most came from units 114 and 112, and our field log records that unit 114 was stuck shut on 7 October. In these episodes saturated RH was a consequence of a sealed chamber rather than a sign of a wet sensor; the closures were flagged automatically and removed as chamber failures (main text Fig. 6a). Because the anomaly is available every hour, stuck lids could also be flagged in real time and fixed in the field.

The other 65 episodes (15 units, 941 h; median 14 h) were wet sensors, mostly during rain, including a 20–22 October event that wetted most units at once. Wet-sensor closures are removed in the main (RH-screened) dataset and kept in the as-deployed dataset. The open-lid baseline recovered within hours of drying (Fig. S7). Of the 16 wet-sensor episodes that ended with the baseline more than 100 ppm above the other units, 15 returned to within 50 ppm 1–3 h after RH fell below 99% (median 2 h); the other was not followed long enough to tell. Recovery time did not depend on episode length (Spearman $\rho = 0.37$, $p = 0.17$). During episodes, only 12–26% of wet hours had an anomaly above 100 ppm, and this share did not grow with episode length.

The effect on flux was larger. The Fluxbot/autochamber ratio was 0.77 in the first 2 h of an episode and 0.58 after 13–24 h, against 0.99 in dry periods more than 72 h from any wet hour, so the main field effect of a wet sensor was a depressed slope rather than an offset, and it built up over the first day. After drying, the ratio was 0.86 in the first 3 h and about 0.85 through the first day, and then varied around the dry-period ratio of 0.99 (0.8–1.05) on the second day as fewer episodes contributed (Fig. S7d). Part of this lag may be real, because soils were re-equilibrating after rain and the collars of the two systems may respond differently; however, these data cannot separate the two.

Wetting left no lasting effect: a unit's dry-period flux ratio did not change with its cumulative wet hours (+0.8% per 100 wet hours, $t = 0.09$). Water also did not cause recording failures: missed recordings were less frequent in the 6 h after a wet hour (7% against 26%), because outages clustered in the dry battery-depletion period, and error codes were rarer in wet hours (0.9% against 1.7% of readings).

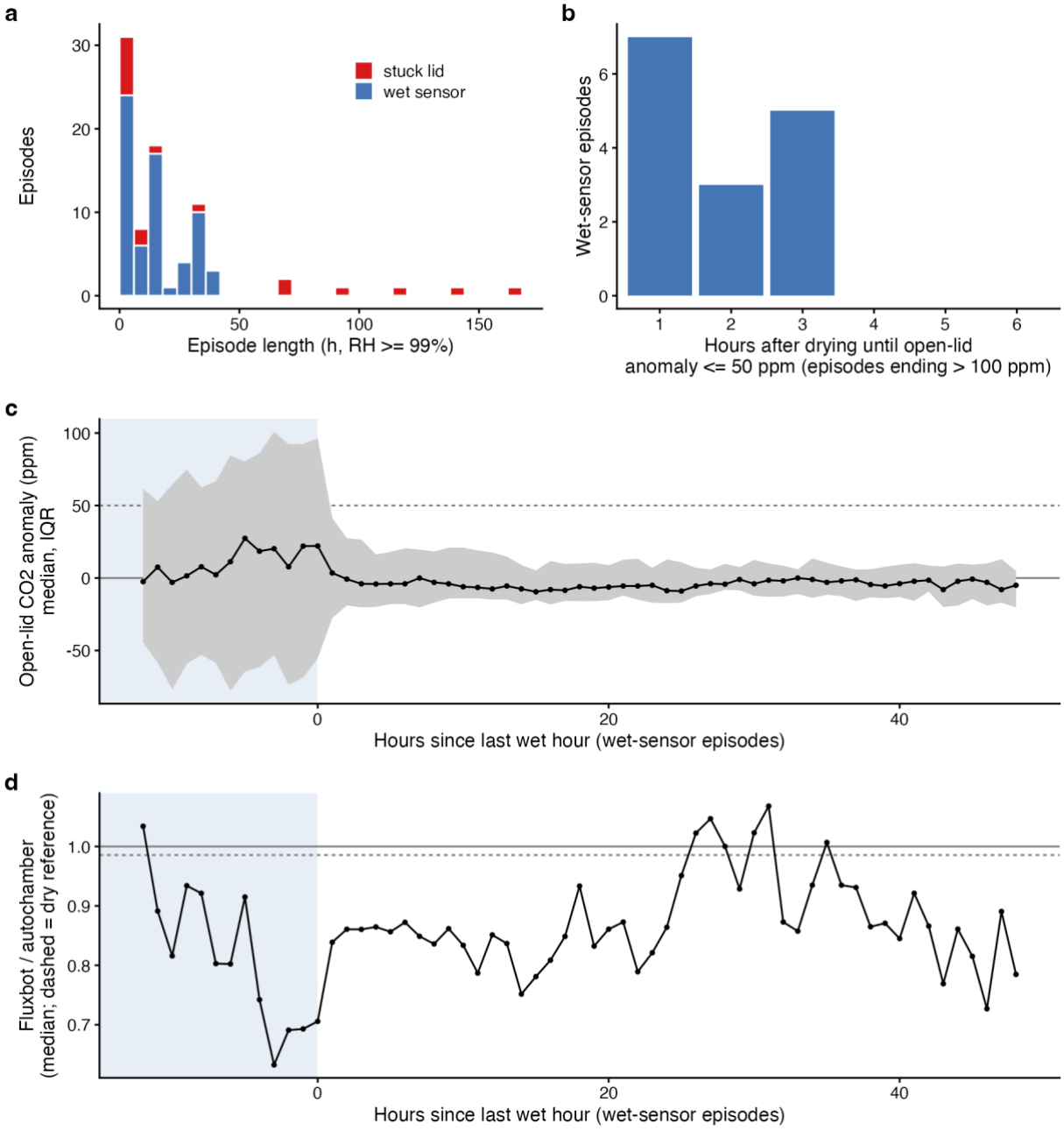


Fig. S7. *Wet sensors in the field. (a) Lengths of episodes with in-chamber RH ≥ 99%, split into stuck lids and wet sensors. (b) Hours after drying until the open-lid baseline returned to within 50 ppm of the other units, for wet-sensor episodes that ended more than 100 ppm high. (c) Open-lid baseline anomaly (median, IQR) and (d) Fluxbot/autochamber flux ratio (median), relative to the last wet hour; dashed line in (d): dry-period reference.*

S4.3 Data loss and bias from moisture

Removing wet-sensor closures to form the main (RH-screened) dataset excluded 661 closures (main text Fig. 6a). The offset was −3.0% over 357 as-deployed compared hours and −0.3% over 305 RH-screened compared hours; hourly r was 0.69 and 0.72, and daily r 0.80 and 0.85 (Table S2b). Keeping stuck-lid

closures, which are removed as chamber failures in the main dataset, lowered the offset to −7.1%. Removing a further 1–24 h after each wet episode moved the offset to as much as +4.1% and cost up to 18% more closures without improving hourly r. The monthly budgets agreed in both the RH-screened and the as-deployed datasets, with Fluxbot/autochamber ratios of 0.98 (95% CI 0.81–1.18) and 0.96 (0.77–1.21); in both, the width of the intervals reflects differences among collars rather than between systems.

Removing wet periods can also bias a budget through the hours it removes. The autochambers record whether or not the Fluxbots are wet, so they show what the soil did in the hours the Fluxbots lose. In stand-hours in which more than half of the recording Fluxbots were wet (stuck-lid closures excluded), autochamber fluxes were 3% above a model of flux on temperature and time of day; when no Fluxbots were wet, they were 1% below it. Wet periods were therefore modestly high-flux periods, plausibly because of rewetting pulses. Removing them does not bias the hourly comparison, in which both systems are compared over the same hours, but a gap-filled budget depends on which hours carry data. Keeping only the autochamber stand-hours in which the Fluxbot array had a stand mean (Fluxbot coverage), and gap-filling the remaining hours in the same way, lowered the autochamber budget by 0.7% under as-deployed coverage and 1.3% under RH-screened coverage. The additional restriction from screening accounts for about 0.6 percentage points. Screening out wet sensors therefore removes a measurement bias at the cost of a small sampling bias in budgets.

S5. Temperature response and resilience

S5.1 Diel cycle and temperature response

The hour-of-day curves of the two systems were correlated (r = 0.70). With model selection, Fluxbot fluxes were elevated from 17:00 to midnight with a nominal peak at 21:00. With LM fits they peaked at 17:00, closer to the autochamber peak at 18:00, because model selection raises fluxes most in the evening, when curvature is strongest (Section S2.3). Fluxbot fluxes were also higher relative to autochamber fluxes when the air was warmer than the soil: the Fluxbot/autochamber ratio increased by 3.4% for each °C by which air temperature exceeded 10-cm soil temperature. Chamber heating is unlikely to explain this, because air inside a closed Fluxbot warmed by only 0.06 °C during a closure.

Q_{10} was estimated in two ways over the stand-hours in which both systems reported. First, pooled hourly fluxes (F) of each system were fitted to $F = a \cdot \exp(bT)$ by nonlinear least squares. Second, for chambers with at least 100 qualifying chamber-hours, we fitted $\log F = a + bT$ using fluxes above 0.5 μmol m^{-2} s^{-1}. $Q_{10} = \exp(10 \cdot \text{mean } b)$ is the geometric mean of the chamber Q_{10} values, and we resampled chambers within stands for the ratio interval. Pooled fits gave a Q_{10} of 2.84 (95% CI 2.72–2.97) for autochambers

and 3.70 (3.47–3.94) for Fluxbots; these intervals treat individual fluxes as independent. Chamber-level Q_{10} ranged from 2.0 to 3.6 among autochambers and from 1.3 to 10.9 among Fluxbots (values for each chamber are in the data release). Geometric mean chamber Q_{10} was 2.80 (2.51–3.12) and 3.58 (2.86–4.51), respectively, a ratio of 1.28 (1.00–1.64; t-test $p = 0.14$), or 1.21 without the two most extreme Fluxbots.

Because soil temperature and flux both declined over the month, the temperature response can be confounded with season. As a check, we repeated the chamber-level fits, with fluxes above 0.3 μmol m^{-2} s^{-1}, adding a linear seasonal trend and the log of 72-h precipitation as covariates. Q_{10} was then 2.40 for autochambers and 3.69 for Fluxbots ($p = 0.12$ for the difference). Air temperature explained Fluxbot fluxes better than 10-cm soil temperature (ΔAIC = 28), whereas soil temperature was much the better driver for autochambers (ΔAIC = 2,039 in its favor).

S5.2 Resilience

Mean Fluxbot unit success was 60% in stand 1 and 49% in stand 2, and at least three units reported in 81% and 70% of hours, respectively. The longest outages with no Fluxbot unit reporting were 25 h in stand 1 and 47 h in stand 2 (main text Fig. 6d). For autochambers, mean unit success was 66% in stand 1 and 89% in stand 2, and replicated coverage 67% and 90%. Fig. S8a shows the record of every chamber. Autochamber losses came as blocks affecting a whole array at once, most clearly the 164 h in which the stand-1 array produced no data, whereas Fluxbot losses were spread across individual units, apart from the start of the deployment and the battery depletion on 16–18 October, which affected all units.

In both systems, stand-hours with fewer than three units reporting were more frequent than expected if units had failed independently. For stand-2 Fluxbots, 30% of hours had fewer than three units, against 13% expected from each unit's own hourly success rate (a Poisson-binomial distribution); for stand-1 autochambers, 33% against 11% (Fig. S8b). In the autochambers this reflects the shared pneumatics and power; in the Fluxbots, a battery depletion across all units on 16–18 October, after they had been deployed and recharged together. Staggered or solar recharging would make Fluxbot failures closer to independent.

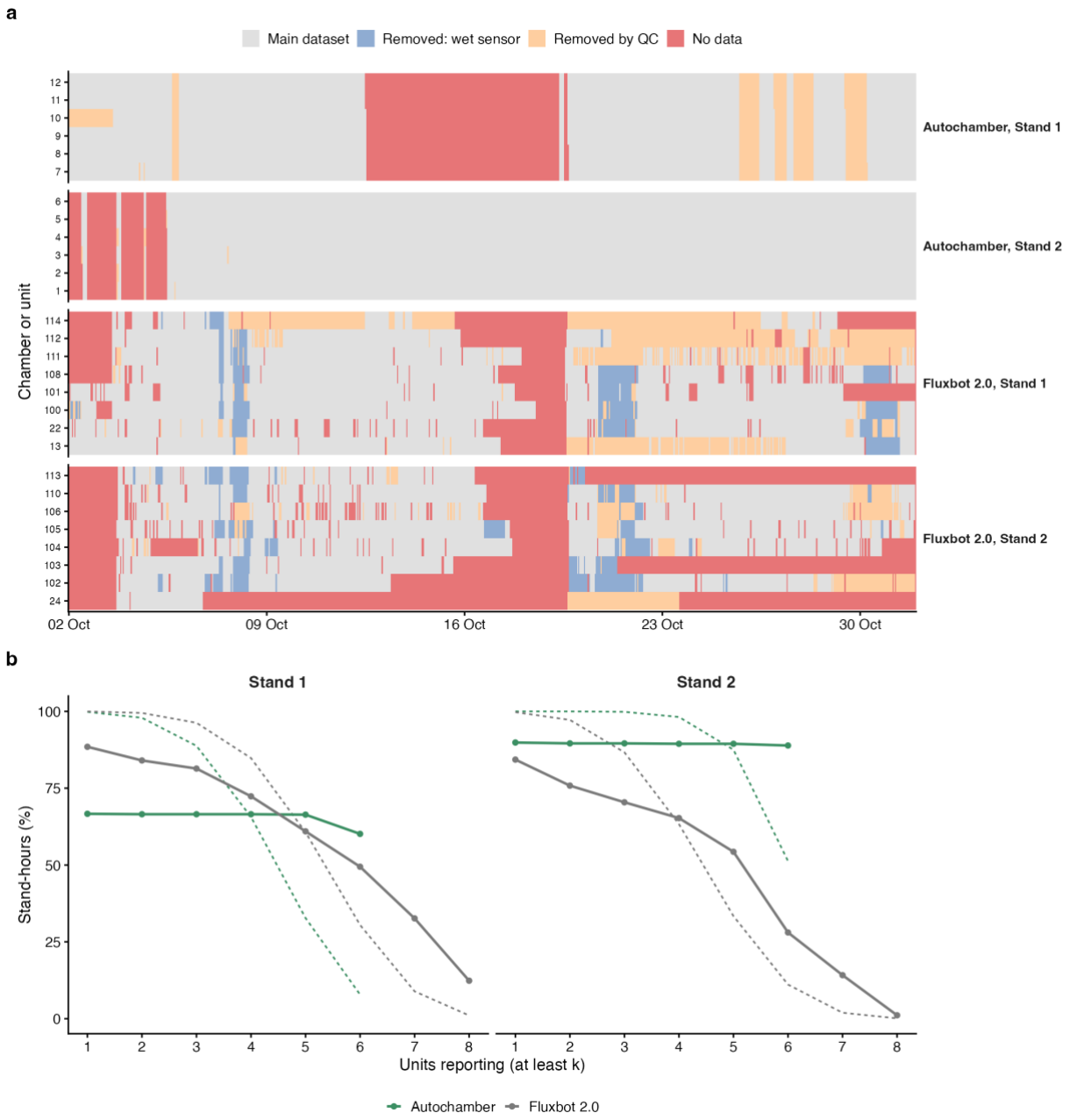


Fig. S8. *Data record and resilience. (a) Every chamber, every hour, colored by what happened to its data: in the main dataset, removed as a wet sensor, removed by quality control, or no data (colors as in main text Fig. 6a); an autochamber hour counts as in the main dataset if either of its two closures is. (b) Replicated coverage: percentage of stand-hours with at least k units reporting, observed (solid) and expected if units failed independently (dashed), by stand and system.*

References

[dataset] Finzi, A., Keiser, A., Giasson, M.-A., Nieland, M., 2026. Soil carbon in a hemlock stand infected by hemlock woolly adelgid at Harvard Forest since 2015. Harvard Forest Data Archive: HF293 (v.10). Environmental Data Initiative. https://doi.org/10.6073/pasta/a4ebf6b3eb19d832fcf09c81ec6dfa73.

Hüppi, R., Felber, R., Krauss, M., Six, J., Leifeld, J., Fuß, R., 2018. Restricting the nonlinearity parameter in soil greenhouse gas flux calculation for more reliable flux estimates. PLoS ONE 13, e0200876. https://doi.org/10.1371/journal.pone.0200876.

Hutchinson, G.L., Mosier, A.R., 1981. Improved soil cover method for field measurement of nitrous oxide fluxes. Soil Science Society of America Journal 45, 311–316. https://doi.org/10.2136/sssaj1981.03615995004500020017x.

Pan, C., Patel, V., Gewirtzman, J., Richardson, I., Dubey, R., Caylor, K., Dollar, A., Forbes, E., 2024. Fluxbot: the next generation – design and validation of a wireless, open-source mechatronic CO2 flux sensing chamber, in: Proceedings of the 7th ACM SIGCAS/SIGCHI Conference on Computing and Sustainable Societies. ACM, New York, pp. 85–96. https://doi.org/10.1145/3674829.3675063.

Rheault, K., Christiansen, J.R., Larsen, K.S., 2024. goFlux: a user-friendly way to calculate GHG fluxes yourself, regardless of user experience. Journal of Open Source Software 9, 6393. https://doi.org/10.21105/joss.06393.

Schuirmann, D.J., 1987. A comparison of the two one-sided tests procedure and the power approach for assessing the equivalence of average bioavailability. Journal of Pharmacokinetics and Biopharmaceutics 15, 657–680. https://doi.org/10.1007/BF01068419.